Thio and selenosilicates, sulfide and selenide counterparts of silicates: similarities and differences

Annie Pradel, Andrea Piarristeguy

▶ **To cite this version:**

Annie Pradel, Andrea Piarristeguy. Thio and selenosilicates, sulfide and selenide counterparts of silicates: similarities and differences. Comptes Rendus. Géoscience, 2022, 354 (S1), pp.1-21. 10.5802/crgeos.109 . hal-03797612

HAL Id: hal-03797612
https://hal.science/hal-03797612

Submitted on 16 Nov 2022

HAL is a multi-disciplinary open access archive for the deposit and dissemination of scientific research documents, whether they are published or not. The documents may come from teaching and research institutions in France or abroad, or from public or private research centers.

L'archive ouverte pluridisciplinaire **HAL**, est destinée au dépôt et à la diffusion de documents scientifiques de niveau recherche, publiés ou non, émanant des établissements d'enseignement et de recherche français ou étrangers, des laboratoires publics ou privés.

Thio and selenosilicates, sulfide and selenide counterparts of silicates: similarities and differences

A. Pradel*, A. Piarristeguy

ICGM, Univ Montpellier, CNRS, ENSCM, Montpellier, France.

* corresponding autor : annie.pradel@umontpellier.fr

Postal address: **ICGM - UMR 5253, CC 043, 1919 route de Mende, 34293 Montpellier - France**

Phone number: --

Abstract

Thiosilicate and selenosilicate glasses are the sulfide and selenide counterparts of the well-known silicate glasses. The paper reviews the main investigations carried out to shed light on the structural, thermal and electrical characteristics of these glasses, showing their particularities compared to their oxide counterparts, such as a more complex structure with the presence of both, corner and edge-sharing tetrahedra and much higher ion conductivity due to the larger polarizability of the chalcogen and the more covalent nature of the bonds, but also, their similarities with the presence of both, bridging and non-bridging S or Se or the existence of a mixed alkali effect when two mobile Li^+ and Na^+ cations co-exist in the glassy network. Structural consequences of competition between SiS_2 and another former, GeS_2, $PS_{5/2}$ or $BS_{3/2}$ are also discussed.

Keywords thiosilicate, selenosilicate, edge-sharing tetrahedron, mixed alkali effect, glass former competition, glass structure, solid electrolyte

1. Introduction

In the mid-sixties, a consequent research effort has been devoted to the study of new materials with potential interest as solid electrolytes. At the time, focus was put on crystalline compounds. Very remarkable compounds were found such as sodium β-alumina, $RbAg_4I_5$, NASICON (Sodium Superionic Conductor). No much interest was deserved to glasses since the conductivity of ion conducting glasses, the only known ones being oxides, was rather poor. The

situation changed in the late seventies with the publication of the "Weak Electrolyte Theory" (WET) (Ravaine, 1977).

In this model, the glass is treated as a weak electrolyte with the glass former compound, e.g. SiO_2, being the solvent and the modifier compound, e.g. Na_2O, being the solute, such assumption being supported by the fact that glasses have very low dielectric constants (ε_r ~5-10 in oxide glasses). The authors have established experimentally that the electrical conductivity of xNa_2O-$(1-x)SiO_2$ glasses varied as the square root of their thermodynamic activity. And, with the assumption of a weak dissociation, so does the concentration of ions Na^+ resulting from the dissociation of the modifier compound ($Na_2O \leftrightarrow Na^+ + NaO^-$). Therefore, the conductivity varies as the concentration of these "free" ions. The authors proposed that the only charge carriers free to move throughout the glassy matrix in the presence of an electric field were those released as a result of the solute dissociation. A larger solute dissociation would then result in a larger number of free charge carriers, and subsequently in a larger conductivity.

According to the WET, the ionic conductivity in a glass is then closely related to the dielectric permittivity of the medium and will increase with increasing this parameter. Therefore, the replacement of oxygen by a more polarisable atom, such as S, or Se, was supposed to increase the conductivity. The first Na^+ conducting thiogermanate glasses were then synthesized (Barrau, 1978). In the following years, owing to the success of the WET, ion conducting glasses based upon other sulfide networks such as thioborate (Levasseur, 1981), thiophosphate (Mercier, 1981), thioarseniate (Visco, 1985) and thiosilicate networks (Akridge, 1984; Pradel, 1986; Sahami, 1985) were investigated.

It was the first time that these families, sulfide counterparts of the very well-known silicate, germanate, borate and phosphate glasses were elaborated. At the time, simple glasses comprising a network and a modifier were prepared. Later, more complex systems were elaborated in order to investigate famous effects, largely debated in the oxide family, such as the mixed alkali effect (MAE), the mixed glass former effect (MFE). The motivation of these investigations being the search for fast ion conductors, literature reports mainly on glass systems comprising Li^+ and Na^+ as mobile cations.

In this paper, we will only focus on thiosilicate and selenosilicate glasses, and report their preparation, structural, thermal and electrical characterization, showing their particularities compared to their oxide counterparts due to the larger polarizability of the chalcogen and the more covalent nature of the bonds but also, their similarities with the existence of both, bridging

and non-bridging anions or the non-linear variation of properties when two mobile cations co-exist in the glassy network.

2. Elaboration of thio and selenosilicate glasses

Like their oxide counterparts, thiosilicate and selenosilicate glasses can be prepared as bulk materials, powders or thin films. On the other hand, and in contrast to oxides, their preparation requires an oxygen-free atmosphere. After preparation, the glasses must be handled in moisture-free glove box since they are highly hygroscopic.

The usual way to prepare the glasses is the direct reaction of the constituting elements (for the former **compounds**, Si and S or Se) or the reaction of the constituting modifier **compounds** (e.g. Li_2S), former **compound** (e.g. SiS_2, GeS_2 …) and eventually "dopants" (e.g. LiI) mixed in stoichiometric quantities and placed in quartz tubes sealed under vacuum. The mixture is then melted at temperatures usually comprised between 1000K and 1350K, lower than the required temperatures for silicate glasses (T_f SiO_2 = 1983K; T_f SiS_2 = 1373K; T_f $SiSe_2$ = 1243K). Depending upon the ease in vitrifying, the tube is quenched in air or in various liquids that increase the heat dissipation (water, salted water, liquid nitrogen). When preparing alkali conducting chalcogenide glasses, vitreous carbon crucibles are often inserted in the tube in order to avoid contact of the reacting mixture with the quartz tube and thus contamination of the glass by silica (Levasseur, 1981; Pradel, 1986; Robinel, 1983). The vitreous carbon crucible can be replaced by a layer of carbon obtained by pyrolysis of an organic compound such as acetone (Kennedy, 1989a; Zhang, 1990). Sulfur and to a less extend, selenium have high vapor pressures. A slow heating ramp of ~6K/hour (in presence of S or Se) and ~30K/hour (in presence of already prepared modifier, former compounds…) at the beginning of the reaction process is therefore required in order to avoid any risk of explosion of the quartz tube. The heating treatment can include steps with constant temperature for several hours to optimize the reaction.

Many glasses in the systems M_2X-SiX_2- YX_n-MZ, M = Li, Na, Ag; X = S, Se; Y = Ge, Al, B, P; Z = Cl, Br, I; n = 2, 3/2, 5/2 were prepared in this way, (Kennedy, 1988; Kennedy, 1989a; Levasseur, 1981; Ribes, 1979).

However, thiosilicate glasses, even binary SiS_2 and $SiSe_2$ glasses, have a high tendency to crystallization. Therefore, faster quenching techniques were developed to produce glasses in larger (often, alkali-rich) composition domains. Several techniques can be considered from the simple crush of a droplet between two plates to more sophisticated techniques such as twin roller quenching. In this technique, droplets of molten material are pushed between rotating

twin rollers, giving 50-80 µm thick glassy flakes. The technique allows obtaining quenching rates of about 10^6K/s (Pradel, 1985). Glasses of the system xLi_2S-$(1-x)SiS_2$ were prepared in this way up to large modifier content (x = 0.6) (Pradel, 1986). Several series of thiosilicate and selenosilicate glasses were obtained in such a way (Aotani, 1994; Deshpande, 1988a; Deshpande, 1988b; Michel-Lledos, 1992; Pradel, 1995; Pradel, 1986; Tatsumisago, 1996).

An alternative way to prepare thiosilicate glasses, i.e. the mechanical milling technique, has been proposed by Morimoto in 1999 (Morimoto, 1999). Powders of the starting (former, modifier …) compounds are placed in a jar with a series of balls. The mechanical milling treatment is carried out on the mixture using a planetary ball mill. The mechanical energy transferred to the powder due to collision with the balls allows the reaction between the components of the mixture. Optimization of different parameters such number and size of the balls, rotation speed, allowed the synthesis of $0.6Li_2S$-$0.4SiS_2$ fine powders with similar properties than the melt-quenched samples. An advantage of this method is its ability to proceed at room temperature.

Finally, thin films of several thiosilicate glasses, i.e. Li_2S-SiS_2, Li_2S-SiS_2-LiI, Li_2S-SiS_2-P_2S_5-LiI, were obtained by thermal evaporation of the bulk glasses, which required the development of a specially designed device installed in a glove-box under a controlled argon atmosphere (Creus, 1989). Amorphous films were obtained and further used as solid electrolytes in exploratory research for microbattery development (Creus, 1992). Owing the difficulties to prepare and handle thin films in controlled atmosphere, very few experiments of this type were carried out but one can note a recent work on thiogermanate glasses by Seo and co-workers who prepared films by magnetron sputtering of a glassy target in an Ar atmosphere (Seo 2016).

3. Network formers

Any thiosilicate/selenosilicate glass comprises SiS_2/$SiSe_2$ as the network former compound.

In contrast to SiO_2 which structure comprises a 3D network of corner-sharing (CS) tetrahedra (Td), whatever the considered polymorph (quartz, trydimite, cristobalite), **SiS_2, in its unique known crystalline form, has a structure comprising infinitive chains of edge-sharing (ES) tetrahedra** (figure 1) (Zintl 1935). The situation is more complex in $SiSe_2$ since, in addition to the usually reported polymorph, (named 700-$SiSe_2$ hereafter) isotype of SiS_2 (Hillel, 1971; Peters, 1982; Weiss, 1952), two other polymorphs, prepared by solid state reaction at 400°C and 500°C (named 400-$SiSe_2$ and 500-$SiSe_2$ respectively), have been identified (Pradel, 1993).

The vitreous counterparts of crystalline **SiS_2 and $SiSe_2$ (named $SiS(e)_2$ hereafter)** can be prepared by conventional melt-quench technique even though they have a high tendency to crystallize. **In the silicon sulfide and selenide families it is also possible to produce non-stoichiometric glasses, i.e. Si_xS_{1-x} and Si_xSe_{1-x}, which is not the case in the oxide family counterpart (Tenhover, 1983a; Griffiths, 1984; Johnson, 1986). This is based on the possibility of forming homopolar S(e)-S(e) and Si-Si bonds. Indeed, in these families, the difference in electronegativity between Si (1.8) and S (2.6)/Se (2.6) is not so large, in contrast with the difference in electronegativity between Si (1.8) and O (3.5) in the oxide family. Therefore, homopolar bonds are not as disadvantaged as they are in oxide glasses. It has to be noted that these differences in electronegativity has a strong consequence on the nature of the chemical bonds in the oxide and sulfide/selenide glasses. In oxide glasses, the chemical bonds have a strong ionic character, and SiO_2 can be considered as being built up with SiO_4^{4-} as the basic building block. In $SiS(e)_2$ glasses, the bonds have a strong iono-covalent character and the building blocks are usually rather written as $SiS(e)_{4/2}$. Of course, both descriptions, i. e. SiO_4^{4-} and $SiS(e)_{4/2}$, are just formal ones; they do not reflect the complex reality of the chemical bonds but clearly emphasized the difference between the two families.**

Raman (Griffiths, 1984; Griffiths, 1985; Pradel, 1993; Sugai, 1987; Tenhover, 1983a; Tenhover, 1983b; Tenhover, 1984; Tenhover, 1985) and ^{29}Si NMR experiments (Moran, 1990; Pradel, 1993; Tenhover, 1988) as well as computer-modeling studies (Antonio, 1988; Gladden, 1987; Gladden, 1989a; Gladden, 1989b; Gladden, 1990) based on neutron-scattering data (Johnson, 1986a; Johnson, 1986b) were carried out in order to get insight in the structure of the sulfide and selenide glasses and the unknown $SiSe_2$ polymorphs. ^{29}Si NMR spectra of the $SiSe_2$ polymorphs and $SiSe_2$ glass are shown in figure 2 (Pradel, 1993). The NMR spectrum of the 700-$SiSe_2$ polymorph shows a single peak at -92.6 ppm which can be assigned to the unique Si site present in the structure and involved in edge-sharing tetrahedra. Similar findings were obtained for crystalline SiS_2 with a single ^{29}Si NMR peak at -19.5ppm (Tenhover, 1988). The spectra of 400-$SiSe_2$ and 500-$SiSe_2$ polymorphs are more complex. The first one shows two peaks at -83.5ppm and -63.0 ppm and the second one four peaks at -88.4 ppm, -61.6 ppm, -56.3 ppm and -27.3 ppm. The spectrum of glassy $SiSe_2$ shows three broad peaks at -86.0 ppm, -62.6 ppm, -28.7 ppm, similar to ^{29}Si NMR spectrum of vitreous SiS_2 where the peaks appear at -16.8ppm, -7.6 ppm and +7.5 ppm (Tenhover, 1988). The presence of several peaks in the ^{29}Si NMR spectra of $SiS(e)_2$ compounds suggests the existence of several Si environments. Three

possible Si environments have been suggested: Si belonging to tetrahedra sharing two, one or zero edge(s), shown in figure 3 and labeled E2, E1 and E0 respectively (Antonio, 1988; Gladden, 1987; Gladden, 1989a; Gladden, 1989b; Gladden, 1990; Griffiths, 1984; Griffiths, 1985; Moran, 1990; Pradel, 1993; Sugai, 1987; Tenhover, 1983a; Tenhover, 1983b; Tenhover, 1984; Tenhover, 1985; Tenhover, 1988). For selenide (sulfide) compounds, peaks in the region -80/-90 ppm (-10/20 ppm) are attributed to E2 species, those in region -60/-70ppm (-7/8ppm) to E1 species and E0 species have their signature in region -20/-30ppm (+7/+8 ppm). Therefore, 400-$SiSe_2$ polymorph comprises E2 and E1 species in a ratio 1/1. A tentative structural model that fulfills this requirement is proposed in figure 1 (Pradel, 1993). Both, 500-$SiSe_2$ and vitreous $SiSe_2$ comprise the three species E2, E1 and E0, suggesting a close structural relationship between them. However, a minor discrepancy between E2:E1:E0 ratios (1:2:2 for the crystalline compound compared to 1:2:1 for the glass) exists so, it was suggested that an even better agreement could be achieved if one considered that the glass was comprised of a mixture of the units existing in 400-$SiSe_2$ and 500-$SiSe_2$. It was supported by the fact that the vitreous transition temperature, i.e. the temperature at which the vitreous structure is frozen in, lies around 450°C. All Raman and computer-modeling studies based on neutron diffraction experiments (not described in details here) are consistent with the above findings**, i.e. they confirm the coexistence of E2, E1 and E0 species** (Antonio, 1988; Gladden, 1987; Gladden, 1989a; Gladden, 1989b; Gladden, 1990; Griffiths, 1984; Griffiths, 1985; Moran, 1990; Pradel, 1993; Sugai, 1987; Tenhover, 1983a; Tenhover, 1983b; Tenhover, 1984; Tenhover, 1985; Tenhover, 1988). **On the other hand, they all failed in one way or another to give a complete description of the glass structure that agrees with all experimental data (relative amounts of species for example). Some models such as the random network model by Sugai (Sugai, 1986; Sugai, 1987), are too simplistic. In the cross-linked-chain-cluster (CLCC) model, Griffiths et al. proposed an intermediate range order built up with chain fragments containing E2 units interconnected by E1 and E0 tetrahedra, as shown in figure 4 (Griffiths, 1984). This model was refined by Gladden in an investigation based upon a computer-modeling study of neutron diffraction data (Gladden 1987, Gladden, 1989b). In this work, several types of intermediate range order species were considered, including random chains and the Griffiths CLCC species. The best agreement led to a mixture of 85% random chains containing an average of seven E2 units and 15% of CCLC units, consisting of rings with two E0 and four E2 units each. This model still does not meet all the quantitative experimental constraints imposed by NMR since it underestimates the relative fractions of E1 and E0 units. Later on, Celino and Massobrio used extensive first-**

principle molecular dynamics simulations to describe the atomic structure of $SiSe_2$ (Celino 2005). In this case, it is the relative fraction of E2 that was underestimated. The dominant structural motifs were Si-triads comprising E0 and E1 species and chains fragments of E1 species. All these studies indicate that the glasses comprise a complex mixture of motifs including fragments of chains and CLCCs with various fractions of E2, E1 and E0 units. Compared to vitreous SiO_2 which structure comprises corner-sharing tetrahedron and intermediate range order comprises only tetrahedra rings, the structure of sulfide and selenide glasses is much more complex. It comprises edge-sharing tetrahedra and a very complex MRO including chains and rings.

The presence of edge-sharing tetrahedra constitutes a violation of the traditional Zachariasen network model, which explicitly excludes any connectivities different from corner-sharing. It might explain their strong tendency toward crystallization.

4. Network former/Network modifier

4.1 Single modifier

In oxide glasses, addition of a modifier oxide, e.g. Li_2O, Na_2O, in the former oxide SiO_2, creates the well-known non-bridging oxygen (NBO) **and the consequent Qn species of tetrahedrally coordinated silicon bound to a number, n, of bridging oxygen (BO) (n= 4, 3, 2, 1 or 0) as shown in figure 3**. Do similar **non bridging sulfur or selenium (NBS)** exist when a modifier is added to $SiS(e)_2$? In which case, owing to the presence of edge-sharing tetrahedra, **a larger number of** entities, summarized in Figure 3, might be expected. For example, **a E1Q3 entity would be a tetrahedron with 3 bridging sulfur or selenium (BS), 1 NBS** and sharing an edge with its neighbor.

Structural investigation of glasses M_2X-SiX_2 (M = Li, Na, Ag to a less extent; X = S, Se) was carried out using many complementary characterization techniques including Raman, IR, ^{29}Si, ^{23}Na, ^{7}Li NMR (Pradel, 1995), XPS (Foix, 2001; Foix, 2006) and neutron diffraction (Lee, 1997). No technique alone could give a complete pattern of the structure at local and intermediate orders. However, their combination helped in getting a clear, even though yet incomplete picture.

Information on glass structure can be obtained by comparing data obtained for glasses with those for crystalline model compounds. On this basis, crystallized thiosilicate compounds in the system Na_2S-SiS_2, where crystallographic data are numerous (Cade, 1972; Olivier-Fourcade, 1972; Olivier-Fourcade, 1978), have been used to understand ^{29}Si NMR spectra of

Na_2S-SiS_2, Li_2S-SiS_2 and Ag_2S-SiS_2 glasses (Eckert, 1989; Pradel, 1995). The main information of this investigation can be summarized as follows. For all of the alkali-containing system, the spectra are dominated by two principal resonances in the chemical shift regions 1-7 ppm and -7 to -12 ppm, as shown in figure 5 for the Li_2S-SiS_2 system. The first one is the signature of E0 entities, with no edge-shared with neighbors; the second is the signature of E1 entities with a single edge-shared with neighbor. At low modifier content (10% Li_2S), still remains some E2 entities, which signature occurs at ~ -20ppm. Addition of modifier results in the preferential destruction of edge-sharing tetrahedra, this tendency being much stronger for Li_2S than for Na_2S, 23% E1 remaining in $0.5Li_2S$-$0.5SiS_2$ against 50% E1 (48% according to Watson et al. (Watson, 2017)) in $0.5Na_2S$-$0.5SiS_2$. Note-that no edge-sharing tetrahedra exists in the related Ag_2S-SiS_2 glasses (Pradel, 1995). Owing to the very small ^{29}Si chemical shift variations for thiosilicates, ^{29}Si NMR cannot give direct and straightforward information on BS and NBS presence and distribution. In a recent re-investigation of the structure of Na thiosilicate glasses, complementary deconvolution of both ^{29}Si NMR and Raman spectra was used to extract this information (Watson, 2017). XPS experiments have also been carried out to study Li and Na thiosilicate glasses (Foix, 2001). Data from XPS core peak analysis for lithium glasses are shown in figure 6. For all glasses (the same applies for Na glasses), a decomposition of the large S_{2p} peak into a minimum of two doublets was necessary in order to fit the experimental curve. These doublets are the signature of BS and NBS, similar to the BO and NBO in oxide glasses. The signal at lower energy was assigned to NBS that are more negative than BS associated with the doublet at higher energy. When the modifier increases, the proportion of NBS simultaneously increases in the glass. A thorough analysis of the XPS data including comparison with XPS spectra of model crystalline compounds has been carried out. Based on these data, Li_2SiS_3 and Na_2SiS_3 clusters were built and a Mulliken population analysis was carried out to investigate the charge distribution of the clusters. The main result of the whole study is the noticeable difference existing between the structures of lithium and sodium thiosilicate glasses, in agreement with NMR results. According to XPS data, this is due to different electronic redistribution over the network when one or the other alkali is added, the sodium addition resulting in a change in the electronic distribution over the entire network, which also affects BS. In oxide glasses, the splitting of 2eV between NBO and BO is larger than the splitting of ~0.9eV between NBS and BS in sulfide glasses. It can be explained by the decreased ionic nature of the bonds in thiosilicate and smaller difference in the electronic density around NB and B atoms. XPS valence band spectra of Li_2SiS_3 and Na_2SiS_3 glasses combined with theoretical calculations have also been carried out (Foix, 2006). The difference

in spectra of Li and Na thiosilicate glasses points for the presence of a majority of corner-sharing tetrahedra in the Li glasses whereas a larger proportion of edge-sharing tetrahedra should be present in the Na glass, in agreement with ^{29}Si NMR studies.

Structural investigation of lithium and sodium selenosilicate glasses and crystalline model compounds was also carried out using mainly Raman and ^{29}Si NMR experiments (Pradel, 1992b; Pradel, 1995). ^{29}Si NMR proved to be very powerful in this case. Indeed, much larger ^{29}Si chemical shifts were observed as compared to sulfide glasses and, therefore, species with different Qn could be discriminated as shown in figure 7 for the Li_2Se-$SiSe_2$ family. It can be seen that the tendency to maintain ES species is lower in selenosilicate glasses than in thiosilicate ones. Indeed, none are left at x= 0.5 for selenosilicates. The combination of absence of ES species and possible discrimination between Qn species gave the opportunity to test different structural models that were much discussed in oxide glasses to identify the population distribution of Qn species, e.g. a completely random "statistical" (Schramm, 1984) or chemically ordered (Dupree, 1984; Grimmer, 1984) distribution. Figure 8 shows the experimental spectrum of $0.6Na_2Se$-$0.4SiSe_2$ glass and the resulting simulated distribution based upon the experimental chemical shifts of Qn sites. The two extreme scenarios can be discarded: While the binary model predicts the presence of Q1 species only, the random model would predict less Q1 species than observed.

On the whole, the structural investigation showed a more complex structure in thio and seleno silicate glasses than in oxide analogs. On the other hand, as it occurs in oxide glasses, the addition of modifier leads to the creation of **non-bridging atoms (here S or Se ones),** even though the Si-S(e) bonds are less ionic than the Si-O ones. The nature of both the modifier and chalcogen have consequences on different aspects of the structure such as the number of ES species and the charge on the atoms.

Physicochemical characterization of these glasses has been carried out in order to understand the influence of the structure on glass properties. Figure 9 shows the evolution of the glass transition temperature T_g with the addition of modifier in glasses xM_2X-$(1-x)SiX_2$ with M= Li, Na, Ag and X = S, Se (Pradel, 1989; Michel-Lledos, 1992; Tenhover, 1983a, Tenhover, 1983b, Tenhover, 1984; Johnson, 1986c). T_g decreases rapidly with the first addition of modifier, then slower, if any, for further addition. A rather large difference between T_g of the sulfide and selenide systems could partly be explained by their structural difference i.e. the larger presence of ES species in the sulfide glasses (Pradel, 1992a). The electrical characteristics (electrical conductivity and activation energy) of xM_2X-$(1-x)SiX_2$ glasses with M= Li, Na, Ag and X = S, Se have been investigated. As an example, figure 10 shows the composition dependence of

room temperature conductivity and activation energy for lithium conducting glasses including oxide ones (Pradel, 1992a; Yoshiyagawa,1982). Sulfide and selenide glasses have comparable electrical characteristics. In contrast, the corresponding oxide glasses have much lower conductivities and much larger activation energies. This can be understood if the main factor that controls ion motion is the anion polarizability, which is comparable for S (7.3) and Se (7.5) and much lower for O (3.1). **As described in the introduction section**, this was predicted by the weak electrolyte theory, which is at the basis of the investigation of these glasses. At this point, another family of thiosilicate glasses, which will not be discussed further in the paper, can be mentioned, i.e. glasses with a "salt", e.g. a lithium halide, dissolved in the matrix (Akridge, 1984; Sahami, 1985; **Kennedy, 1986; Pradel, 1989a**). These glasses show increased conductivity owing to the high polarisability of the anions and increase in numbers of mobile ions. Up to 40% of salt can be dissolved in a glass but it is at the expense of its thermal stability.

4.2 Multi-modifiers

In the previous section, it has been shown that addition of Li_2S or Na_2S to SiS_2 has somewhat different consequences on the glass structure and properties with a stronger tendency for Li^+ ions to destroy the edge-sharing tetrahedra and a charge redistribution over the entire network for Na^+ ions leading to more negative BS and NBS. The question is: what would happen if both Li^+ and Na^+ were introduced in the glass network? Some answers were obtained with the investigation of the series of glasses $0.5(x\ Na_2S\text{-}(1\text{-}x)Li_2S)\text{-}0.5SiS_2$ with $0 \leq x \leq 1$. The structural investigation was only carried out by ^{29}Si NMR (Pradel, 1995). It was shown that, while the two main peaks observed in the binary glasses and related to E0 and E1 species (Figure 5) were still present in all mixed Na/Li glasses, their relative intensity was closer to that observed for the binary lithium glasses, even for the first addition of lithium in the sodium glass (Figure 11). The chemical shifts for the two peaks were intermediate between those measured for the binary glasses, which led to the conclusion of the absence of any preferential association of one type of cations for a specific site E1 or E2.

While the replacement of lithium by sodium in the thiosilicate glasses does not seem to transform the structure drastically, it has drastic consequences on several properties. Dependence of glass transition temperature, T_g, electrical characteristics (conductivity σ and activation energy of conductivity E_σ) and activation energy of the relaxation time T_1, E_{T1}, (measured by ^7Li NMR spectroscopy) on composition are shown in figure 12 (Pradel, 1994). A strong non-linear variation of these characteristics is observed. T_g and σ show a high minimum

at x ~ 0.5, whereas the activation energies E_σ and E_{T1} display a maximum for the same values of x. These features are the signature of the mixed alkali effect (MAE), a very well-known phenomenon, reported many times in oxide glasses (Day, 1976; Ingram, 1987; Ingram, 1992), in particular in silicate glasses, the oxide counterparts of the glasses described here (Elliott, 1992). MAE occurs when a modifier is substituted by another one, at a constant total modifier content. Therefore, it appears to be a common feature between oxide and chalcogenide glasses, even though reports on MAE in the second family are scarce and concern mainly two systems, the present one and the Ag_2S-Rb_2S-GeS_2 system (here, we should rather call it "mixed cation effect") (Rau, 2001).

The information reported above in section 4 indicates that Li^+ and Na^+ ions do not favor the same sites in thiosilicate glasses; in particular, NBS are more negative around Na^+ than in the neighborhood of Li^+. In the Ag_2S-Rb_2S-GeS_2 system, it has been clearly demonstrated by EXAFS experiments that the Ag^+ and Rb^+ cations maintained their own environment in the mixed glasses. A similar situation probably applies to the Li/Na thiosilicate glasses. So it can be anticipated that for an ion, to hop from one site to the next is more difficult in a mixed environment than in single alkali one where all the sites are similar and match the only mobile ion. The mobility would then be restricted, which would induce a lower conductivity and higher activation energy as observed.

5. Effect of a competitive network former on thiosilicate glasses

5.1 Thio-aluminosilicate

The glass forming ability of compositions belonging to the Li_2S-Al_2S_3-SiS_2 system, sulfide counterparts of lithium aluminosilicates, has been investigated (Deshpande, 1988b; Hayashi, 2004; Martin, 1991; Pradel, 1992a). The explored region and vitreous domain extension, which depends upon the elaboration technique, i.e. conventional melt-quenching, twin-roller quenching and mechanical alloying, is shown in figure 13. Compared to the oxide family, the glass forming ability is poor with a maximum ratio Al/Li much below 1.5 reported for oxide glasses.

Raman and ^{29}Si, ^{27}Al NMR investigation helped in getting some insights in the structure of these glasses. Raman spectra of glasses $0.5Li_2S$-xAl_2S_3-$(0.5-x)SiS_2$ with x = 0, 0.1, 0.25, along with the spectra of crystalline SiS_2 and crystalline α-Al_2S_3 are shown in figure 14 (Pradel,

1992a). The low temperature form of crystalline Al_2S_3, α-Al_2S_3, has a lacunar wurtzite structure with aluminum occupying tetrahedral sites, a difference with the low temperature form of crystalline Al_2O_3 where aluminum is in an octahedral environment. The main band in the Raman spectrum at 248 cm^{-1} is assigned to the symmetric valence vibrations of the $AlS_{4/2}$ tetrahedron. The main band in the Raman spectrum of crystalline SiS_2 at 427 cm^{-1} can be assigned to the symmetric valence vibrations of edge-sharing $SiS_{4/2}$ tetrahedra. (Tenhover, 1983a) while the two main bands in the Raman spectrum of glass $0.5Li_2S$-$0.5SiS_2$ (x=0) at 408 cm^{-1} and 390 cm^{-1}, are attributed to the stretching vibrations of bridging Si-S bonds or non-bridging $Si-S^-$ bonds. The addition of Al_2S_3 in vitreous $0.5Li_2S$-$0.5SiS_2$ leads to the relative decrease in intensity of the band at 390 cm^{-1} compared to that at 408 cm^{-1} and the simultaneous appearance and further increase of a band at 260 cm^{-1}, which can be attributed to the stretching vibrations of Al-S bonds. Compared to the crystalline compound, the band attributed to Al-S bonds is displaced toward high frequencies, consistent with a shortening of the bonds and therefore, leading to discard an octahedral coordination for the aluminum. It is in agreement with the results from ^{27}Al NMR experiments (Martin, 1991). In this case, the NMR spectra of all prepared Li_2S-Al_2S_3-SiS_2 glasses show a single peak at 110 ppm, similar to the peak present in the NMR spectrum of crystalline α-Al_2S_3. In this case, one expects the lithium to act as a charge compensator and therefore, a decrease in the number of non-bridging sulfur, consistent with the decrease in the band at 390 cm^{-1} in the Raman spectra.

This assumption is supported by the increase of the glass transition temperature T_g with the Al_2S_3 content in the $0.5Li_2S$-xAl_2S_3-$(0.5-x)SiS_2$ glasses as shown in figure 15. It is consistent with an increasing polymerization of the network due to the disappearance of non-bridging sulfur. Such an increase of T_g with increasing the Al_2S_3 content in the glasses has been reported for other series of compositions such as series where the ratio Li/Al was constant and equals to 2/1, 1/1, 1/2 (Martin, 1991).

The electrical properties of Li_2S-Al_2S_3-SiS_2 glasses have been reported. The conductivity σ and activation energy of conductivity E_σ for the $0.5Li_2S$-xAl_2S_3-$(0.5-x)SiS_2$ glasses are shown in figure 15. The slight decrease in σ and increase in E_σ with the addition of Al_2S_3 point for a lower mobility of the lithium acting as charge compensator as compared to lithium close to a non-bridging sulfur. Such assumption is supported by the fact that, in the series yLi_2S-$0.1Al_2S_3$-$(0.9-y)SiS_2$, the conductivity increases from 3.3 10^{-6} $S.cm^{-1}$ to 1.3 10^{-4} $S.cm^{-1}$ when y changes from 0.3 to 0.6.

5.2 Thio-germanosilicate

The structure of $Si_xGe_{1-x}S_2$ glasses has been investigated by analyzing Raman experiments (Tenhover, 1983b). It was shown that, whatever x, separate clusters of the two formers were obtained, which was attributed to the impossible mixing of SiS_2 and GeS_2 networks that adopt different medium-range order configurations: dominance of edge-sharing tetrahedra as shown in section 3 for the first one and dominance of corner-sharing tetrahedra for the second one (Feltz, 1985).

The glass forming ability and properties of glasses, which composition lies along two lines of the system Li_2S-SiS_2-GeS_2, i.e. $0.3Li_2S$-$0.7[(1-x)SiS_2$-$xGeS_2]$ and $0.5Li_2S$-$0.5[(1-x)SiS_2$-$xGeS_2]$ with $0 \leq x \leq 1$, were also investigated (figure 16) (Deshpande, 1988a; **Pradel, 1989b**; Pradel 1998). The glass elaboration required the use of the twin-roller quenching technique. Main structural information was obtained by a Raman experiment analysis. Raman spectra of $0.3Li_2S$-$0.7[(1-x)SiS_2$-$xGeS_2]$ glasses are shown in figure 17. The spectra of the end-line compounds, $0.3Li_2S$-$0.7SiS_2$ and $0.3Li_2S$-$0.7GeS_2$ are dominated by the stretching vibrations of bridging Si-S (Ge-S) bonds and non-bridging $Si\text{-}S^-$ ($Ge\text{-}S^-$) bonds at 412 cm^{-1} (338cm^{-1}) and 368 cm^{-1} (395cm^{-1}) respectively (Souquet,1981). When considering the general evolution of the spectra, three different domains can be identified: For the first substitutions of a glass former by the other one, i.e. for $0 \leq x < 0.50$ and $0.64 < x \leq 1$, a smooth change in the spectra is observed. A sudden change occurs when the Si/Ge ratio is close to 1, i.e. for $0.5 \leq x \leq 0.64$. For $x = 0.5$ the spectrum narrows and the main peak suddenly shifts to higher frequency, close to the frequency of the stretching vibrations of non-bridging $Si\text{-}S^-$ bonds in $0.5Li_2S$-$0.5SiS_2$ glass (377 cm^{-1}). The two spectra look very much alike, but with a broadening for the mixed glass due to the presence of Ge-S bonds, which also explains the further broadening of the spectra upon further GeS_2 addition. The situation is different in the second series of mixed glasses, i.e. $0.5Li_2S$-$0.5[(1-x)SiS_2$-$xGeS_2]$. In this case, a smooth evolution of the Raman spectra (not shown here, Deshpande, 1988a) is observed all along the line from $x = 0$ to $x = 1$. SAXS experiment on the first series $0.3Li_2S$-$0.7[(1-x)SiS_2$-$xGeS_2]$ were carried out in order to check the homogeneity of the glasses (Pradel, 1998). Samples from the three regions were tested. Typical results are shown in the inset of figure 17. Data obtained for samples belonging to the limiting regions ($0 \leq x < 0.50$ and $0.64 < x \leq 1$) could be fitted in the framework of the Debye- Buëche model (Debye, 1949) and therefore, are homogeneous. In contrast, the higher scattering observed for glasses belonging to the central region ($0.5 \leq x \leq 0.64$) rather obeys Porod's law (Porod, 1982), which indicate the presence of aggregates (of about 50Å) in the glass. Both

Raman and SAXS experiments point towards homogeneous glasses in the limiting regions and the occurrence of a phase separation in the central one, leading probably to entities with a composition close to GeS_2 embedded in a matrix which composition is close to that of $0.5Li_2S$-$0.5SiS_2$ glass, i.e. Li_2SiS_3.

Vitreous transition temperatures T_g and density ρ were measured and are shown in figure 18 while the electrical conductivity σ and corresponding activation energy E_σ are shown in figure 19. A smooth evolution of T_g, σ and E_σ when SiS_2 is substituted by GeS_2 is observed for the $0.5Li_2S$-$0.5[(1-x)SiS_2$-$xGeS_2]$ glasses, which agrees with Raman data. In contrast, sudden changes in all parameters ρ, T_g, σ and E_σ occur in the central region for compositions pointed as phase-separated from SAXS and Raman experiments. Appearance of two T_g and lowering of ρ strongly support the presence of a phase separation. Moreover, the larger conductivity of the glasses in the central region, close to the conductivity of the $0.5Li_2S$-$0.5SiS_2$ glass, supports the structural scheme suggested by Raman data, i.e. GeS_2 aggregates embedded in a Li_2SiS_3 matrix, provided that a percolation threshold is reached.

The differences between the two families of glasses, homogeneity versus phase separation, could be understood by the degree of modification of the matrix, which, upon increase, tends to lead to similar configurations for the two end-line compounds. GeS_2 favors corner-sharing tetrahedra so few, if any, edge-sharing tetrahedra are expected in lithium thiogermanate glasses. For $0.3Li_2S$-$0.7SiS_2$ glass, 34% of tetrahedra in the structure are edge-sharing ones; this number goes down to 23% for $0.5Li_2S$-$0.5SiS_2$ glass (Eckert, 1989). Therefore, mixing of the two end-line compounds is more favorable at high modifier content. It can also be pointed out that a crystalline metathiosilicate phase, Li_2SiS_3, exists (Weiss, 1960), whereas crystalline thiodisilicate, $Li_2Si_2S_5$ ($0.33Li_2S$-$067SiS_2$), does not. The phase separation occurs in the $0.3Li_2S$-$0.7[(1-x)SiS_2$-$xGeS_2]$ with the tendency to produce a glassy phase of composition Li_2SiS_3. On the other hand, homogeneous glasses are obtained for the family $0.5Li_2S$-$0.5[(1-x)SiS_2$-$xGeS_2]$ corresponding to the Li_2SiS_3 composition. This can be related to an investigation on lithium germanosilicate glasses, the oxide counterparts of the present glasses (Otto, 1966). Anomaly in the refractive index of several Li_2O-SiO_2-GeO_2 glasses was indeed explained by the tendency of glasses to phase-separate with one of the resulting phase having the disilicate composition. In contrast, no anomaly was observed for $0.33Li_2O$-$0.67[(1-x)SiO_2$-$xGeO_2]$ glasses corresponding to the exact disilicate composition. A similar situation to ours since, in the oxide glasses, crystalline disilicate phase exists while the metasilicate one does not.

5.3 Thio-phosphosilicate

Investigation of lithium thiophosphosilicate glasses of composition $0.6Li_2S$-$0.4[(1-x)SiS_2$-$xP_2S_5]$ with $0 \leq x \leq 1$ was carried out in the eighties (figure 20) (Kennedy, 1989b, Kennedy 1990). The main information is the anomalous evolution of some properties, e.g. glass transition temperature, when substituting a modifier by the other one, with a change at the particular composition corresponding to a ratio SiS_2:P_2S_5 equals to 2:1, i.e. Si/P = 1. Even though a paper, mainly focused on electrochemical properties of this lithium family, was published very recently (Zhao, 2020), the renewal of interest for the thiophosphosilicate glasses concerns mainly the sodium family, and matches the increasing interest for the development of Na all solid-state batteries. Two series of glasses with composition $0.5Na_2S$-$0.5[xSiS_2$-$(1-x)PS_{5/2}]$ and $0.67Na_2S$-$0.33[xSiS_2$-$(1-x)PS_{5/2}]$, $0 \leq x \leq 1$, were recently investigated (figure 20), based upon experiments carried out by complementary characterization techniques, i.e. IR, Raman, ^{29}Si and ^{31}P NMR, DSC, density measurements (Watson, 2018a; Watson, 2018b). Thorough structural analysis with complete deconvolution of Raman and NMR spectra helped in proposing a picture of the glass structure on the basis of the distribution of the different species likely to exist in the glass, and resulting from disproportionation reactions (Watson, 2018a). The different species and their distribution are shown in figure 21 for the $0.5Na_2S$-$0.5[xSiS_2$-$(1-x)PS_{5/2}]$ glasses. The presence of both P Q0 and Si Q3 in glasses comprising 50 mol% Na_2S indicates that there is unequal sharing of the Na^+ ions between the two glass formers; P taking additional Na^+ to form Q0 units and Si giving up Na^+ to form Q3 structures. For the $0.67Na_2S$-$0.33[xSiS_2$-$(1-x)PS_{5/2}]$ glasses, some complexity is added to the structure since a significant concentration of unreacted Na_2S species are present in all glasses. Densities ρ and glass transition temperatures T_g were measured for all glasses (Watson, 2018b). Their evolution with composition is consistent with the structural models proposed for the glasses. As an example, figure 22 shows the evolution of T_g, molar volume (calculated from experimental ρ) and fraction of BS (BS/(BS + NBS) calculated from the distribution of all species) when P is substituted by Si for $0.5Na_2S$-$0.5[xSiS_2$-$(1-x)PS_{5/2}]$ glasses. T_g remains fairly constant for the first additions of SiS_2 when the structure is still dominated by P Q1 and Q0 species (figure 21). When $x \geq 0.5$, Si Q2 and Q3 species starts being dominant and so, the fraction of BS. Then, T_g starts and keeps on increasing with further addition of SiS_2. At the opposite, the molar volumes decrease with the increase in BS and therefore, with the networking increase through the increase in Si Q2 and Q3 species. Finally, a ^{23}Na NMR investigation of these glasses has been reported recently (Shastri, 2019), which gives information on the dynamics and distribution of Na^+ ions. The most relevant information, suggested by a Na NMR second moments study and related to the glass structure,

is a homogeneous distribution of sodium in the glass network over most of the composition range, but for Na-richest ones where sodium tend to cluster.

5.4 Thioborosilicate

As far as we know, a single composition, i.e. the $0.30Li_2S$-$0.21SiS_2$-$0.09B_2S_3$-0.40LiI glass, has been investigated in the late eighties (Kennedy, 1989a). Nothing has been done in these systems ever since and until very recently when a structural investigation of a series of glasses with composition $0.6Na_2S$-$0.4[(1-x)SiS_2$-$xBS_{3/2}]$, $0 \leq x \leq 1$, has been reported (inset figure 23) (Curtis, 2019). IR, Raman, ^{29}Si and ^{11}B NMR experiments were carried out in order to study the changes occurring in the glass structure when a glass former was substituted by the other one. The structural analysis was similar to the analysis described in the previous section for thiophosphosilicate glasses. In the same way, deconvolution of Raman and NMR spectra helped in proposing a picture of the glass structure on the basis of the distribution of the different species likely to exist in the glass, and resulting from disproportionation reaction. The different species for these thioborosilicate glasses and their distribution are shown in figure 23. In fact, owing to the difficulty to obtain pure B_2S_3 exempt of oxygen, several oxi-sulfide species were present in the glasses. These minority species are not shown in figure 23. The main important information can be summarized as follows. Tetrahedrally coordinated Si with a single BS (Si Q1) are the dominant species in the end-line member, $0.6Na_2S$-$0.4SiS_2$ glass while B Q0 corresponding to 3-coordinated boron with no BS is the dominant one in $0.6Na_2S$-$0.4BS_{3/2}$ glass. Upon substitution, there is a disproportionate sharing of the Na^+ between the B and Si subnetworks with Si taking additional Na^+ to form Si Q0 entities and B giving up Na^+ to form B Q1 species. Once again, it is interesting to note that no crystalline phase with composition $Na_6Si_2S_7$ has ever been reported, while Na_4SiS_4 exists (Cade, 1972; Eckert, 1989). On the whole, it appears that, in multi-former thiosilicate glasses, the thiosilicate subnetwork tends to adopt a configuration close to that of a neighboring crystalline phase.

6. Conclusion

Thio- and selenosilicate glasses are the sulfide and selenide analogs of silicate glasses. Owing to the different characteristics of the chalcogen, e.g. size and polarizability, these glasses show markedly different structures and properties, in particular, a much higher electrical conductivity σ, which attracted attention for the development of lithium and more recently sodium all solid state batteries. The structure of the glass formers, $SiS(e)_2$, is comprised of both edge and corner sharing tetrahedra, a major difference with silica. Upon addition of a modifier, a

depolymerization of the network with appearance of NBS occurs, which is similar to the creation of NBO in silicate glasses. Preferential destruction of edge-sharing tetrahedra is generally observed with an increasing trend in the sequences: S to Se and Na to Li to Ag. Thiosilicate glasses comprising two modifiers show the very-well known mixed alkali effect with a strong decrease in both, T_g and σ for mixed glasses compared to single ones, a common characteristic with silicates. When added to lithium thiosilicate, aluminum sulfide, Al_2S_3, behaves as a former **compound**, which decreases the number of NBS and results in an increase in T_g and slight decrease in σ. The mixed glass former effect, observed when a glass former is replaced by another one, the total amount of modifier being constant, has been investigated in thiosilicate glasses with the second former **compound** being GeS_2, $PS_{5/2}$ or $BS_{3/2}$. Depending upon the amount of modifier, lithium thiogermanosilicate glasses are either homogeneous or phase-separated, with a non-linear variation of properties, e.g. ρ, T_g and σ, in the second case. Trend to phase-separate and produce a subnetwork with composition of an existing crystalline phase has also been reported in the oxide analogs, the germanosilicate glasses. In sodium thiophosphosilicate and thioborosilicate glasses, disproportionation reactions between the two formers occur with the transfer of Na^+ from the Si subnetwork to the P subnetwork in the first family. In contrast, Na^+ are transferred from the B subnetwork towards the Si subnetwork in thioborosilicate glasses. In both case, the resulting composition of the Si subnetwork tends to acquire the composition of an existing crystalline phase, i.e. $Na_4Si_4S_{10}$ corresponding to Si Q3 species and Na_4SiS_4 corresponding to Si Q0 species.

One of the main interests of the investigation of these thio- and seleno-silicate glasses is to shed light on the consequence of a change in the nature of the chemical bonds, from highly ionic in oxides to strongly ionocovalent in sulfides/selenides, on the structure and physicochemical properties of the obtained glasses. Apart from this academic interest, these glasses could get renewal of interest since they could be at the basis of the elaboration of new glass-ceramics to be used as solid electrolytes for the development of sodium all-solid-state batteries.

Acknowledgements

The authors wish to thank Mickaël Bigot for his help in preparing all the figures of the manuscript.

References

569 Akridge, J.R., 1984. US Patent No. 4,465,745
570 Antonio, G. A., Kalia, R. K., Vashishta, P., 1988. $SiSe_2$ glass: A molecular dynamics study. J.
571 Non-Cryst. Solids 106 (1-3), 305-308.
572 Aotani, N., Iwamoto, K., Takada, K., Kondo, S., 1994. Synthesis and electrochemical properties
573 of lithium ion conductive glass, Li_3PO_4-Li_2S-SiS_2. Solid State Ionics 68 (1-2), 35-39.
574 Barrau, B., Kone, A., Ribes, M., Souquet, J. L., Maurin, M., 1978. Synthesis and study of the
575 electrical conductivity of glasses belonging to the sodium monosulfide-germanium disulfide
576 System. C. R. Hebd. Seances Acad. Sci., Ser. C287, 43−46.
577 Cade, A., Philippot, E., Ribes, M., Maurin, M., 1972. Crystal-structure of sodium thiosilicate
578 $Na_4Si_4S_{10}$. C. R. Hebd. Seances Acad. Sci., Ser. C274, 1054-1056.
579 Celino, M., Massobrio, C., 2005. First principles modeling of intermediate range order in
580 amorphous $SiSe_2$. Computational Materials Science 33 (2005) 106-111.
581 Creus, R., Sarradin, J., Astier, R., Pradel, A., Ribes, M., 1989. The use of ionic and mixed
582 conductive glasses in microbatteries. Materials Science and Engineering: B 3(1-2), 109-112.
583 Creus, R., Sarradin, J., Ribes, M., 1992. Thin films of ionic and mixed conductive glasses: their
584 use in microdevices. Solid State Ionics 53-56, 641-646.
585 Curtis, B., Francis, C., Kmiec, S., Martin, S.W., 2019. Investigation of the short range order structures
586 in sodium thioborosilicate mixed glass former glasses. J. Non-Cryst. Solids 521, 119456.
587 Day, D. E., 1976. Mixed alkali glasses -Their properties and uses. J. Non-Cryst. Solids 21 (3),
588 343-372.
589 Debye, P., Buëche, A. M., 1949. Scattering by an Inhomogeneous Solid. J. Appl. Phys. 20, 518-
590 524.
591 Deshpande, V.K., Pradel, A., Ribes, M., 1988. The mixed glass former effect in the Li_2S:SiS_2:
592 GeS_2 system. Materials Research Bulletin 23 (3), 379-384. (Deshpande, 1988a)
593 Deshpande, V.K., Pradel, A., Ribes, M., 1988. Influence of Al_2S_3 on the electrical conductivity
594 of the Li_2S-SiS_2 glass system. Solid State Ionics 28-30, 756-761. (Deshpande, 1988b)
595 Dupree, R., Holland, D., McMillan, P.W., Pettifer, R.F., 1984. The structure of soda-silica
596 glasses: A mas NMR study. J. Non-Cryst. Solids 68 (2-3), 399-410.
597 Eckert, H., Kennedy, J. H., Pradel, A. Ribes, M., 1989. Structural transformation of thiosilicate
598 glasses: ^{29}Si MAS-NMR evidence for edge-sharing in the Li_2S-SiS_2. J. Non-Cryst. Solids
599 113, 287-293.
600 Elliott, S.R., 1992. Nuclear spin relaxation in glassy ionic conductors. J. Phys. IV France 02
601 C2-51-C2-59.

602 Feltz, A., Pohle, M., Steil, H., Herms, G., 1985. Glass formation and properties of chalcogenide
603 systems XXXI. RDF studies on the structure of vitreous GeS_2 and $GeSe_2$. J. Non-Cryst.
604 Solids 69 (2-3) 271-282.
605 Foix, D., Gonbeau, D., Taillades, G., Pradel, A., Ribes, M., 2001. The structure of ionically
606 conductive chalcogenide glasses: a combined NMR, XPS and ab initio calculation study.
607 Solid State Sciences 3, 235-243.
608 Foix, D., Martinez, H., Pradel, A., Ribes, M., Gonbeau, D., 2006. XPS valence band spectra
609 and theoretical calculations for investigations on thiogermanate and thiosilicate glasses.
610 Chemical Physics 323, 606-616.
611 Gladden, L. F., Elliott, S. R., 1987. Computer-generated models of a-$SiSe_2$: Evidence for a glass
612 exhibiting medium-range order. Phys. Rev. Lett. 59 (8), 908.
613 Gladden, L. F., Elliott, S. R., 1989. Computer-generated models of a-$SiSe_2$: I. The algorithm. J.
614 Non-Cryst. Solids109 (2-3), 211-222. (Gladden, 1989a)
615 Gladden, L. F., Elliott, S. R., 1989. Computer-generated models of a-$SiSe_2$: II. Structural
616 studies. J. Non-Cryst. Solids 109 (2-3), 223-236. (Gladden, 1989b)
617 Gladden, L. F., 1990. Computer-modelling studies of 4-2 coordinated glasses. J. Non-Cryst.
618 Solids 123 (1-3), 22-25.
619 Griffiths, J. E., Malyj, M., Espinosa, G. P., Remeika, J. P., 1984. Crystalline $SiSe_2$ and Si_xSe_{1-x}
620 glasses: Syntheses, glass formation, structure, phase separation, and Raman spectra. Phys.
621 Rev. B 30, 6978.
622 Griffiths, J. E, Malyj, M., Espinosa, G.P., Remeika, J.P, 1985. Nonstoichiometric selenium rich
623 Si_xSe_{1-x} films. Solid State Commun. 53(7), 587-590.
624 Grimmer, A.R., Mägi, M., Hähnert, M., Stade, H., Samoson, A., Wicker, W., Lippmaa, E.,
625 1984. High-resolution solid-state ^{29}Si nuclear magnetic resonance spectroscopic studies of
626 binary alkali silicate glasses. Phys. Chem. Glasses 25 (4), 105-109.
627 Hayashi, A., Fukuda, T., Morimoto, H., Minami, T., Tatsumisago, M., 2004. Li_2S-Al_2S_3-SiS_2
628 prepared by mechanical milling. Journal of Materials Science 39, 5125-5127.
629 Hillel, R., Cueilleron, J., 1971. Preparation et etude du seleniure de silicium: $SiSe_2$. Bull. Soc.
630 Chim. France 15(2) 394.
631 Ingram, M.D., 1987. Ionic conductivity in glass. Phys. Chem. Glasses 28 (6) 215-234.
632 Ingram, M. D., 1992. Thermodynamics, Structure, and Structural Dynamics in Glass Progress
633 Report. Ber. Bunsenges. Phys. Chem. 96 (11), 1592-1599.

Johnson, R.W., Price, D.L., Susman, S., Arai, M., Morrison, T.I., Shenoy, G.K., 1986. The structure of silicon-selenium glasses: I. Short-range order. J. Non-Cryst. Solids 83(3), 251-271. (Johnson, 1986a)

Johnson, R.W., 1986. Diffraction isosbestic points and structural systematics in the Si_xSe_{1-x} glass system. J. Non-Cryst. Solids 88 (2-3), 366-380. (Johnson, 1986b)

Johnson, R.W., Susman, S., McMillan, J., Volin, K.J., 1986. Preparation and characterization of Si_xSe_{1-x} glasses and determination of the equilibrium phase diagram. Mater. Res. Bull. 21 (1), 41-47. (Johnson, 1986c)

Kennedy, J.H, Sahami, S., Shea, S., Zhang, Z., 1986. Preparation and conductivity measurements of SiS_2-Li_2S glasses doped with LiBr and LiCl. Solid State Ionics 18-19, 368-371.

Kennedy, J.H., Zhang, Z., 1988. Improved stability for the SiS_2-P_2S_5-Li_2S-LiI glass system. Solid State Ionics 28-30, 726-728.

Kennedy, J.H., 1989. Ionically conductive glasses based on SiS_2. Materials Chemistry and Physics 23 (1-2) 29-50. (Kennedy, 1989a)

Kennedy, J.H., Zhang, Z., 1989. Preparation and electrochemical properties of the SiS_2-P_2S_5-Li_2S glass coformer system. J. Electrochem. Soc. 136 (9) 2441. (Kennedy, 1989b)

Kennedy, J.H., Zhang, Z., Eckert, H., 1990. Ionically conductive sulfide-based lithium glasses. Recent advances in fast ion conducting materials and devices, 155-165.

Lee, J. H., Pradel, A., Taillades, G., Ribes, M., Elliott, S. R., 1997. Structural studies of glassy $(Li_2S)_{0.5}(SiS_2)_{0.5}$ by isotopic-substitution neutron diffraction. Phys. Rev. B 56 (1), 10934.

Levasseur, A., Olazcuaga, R., Kbala, M., Zahir, M., Hagenmuller, P., 1981. Synthesis and electrical-properties of new sulfide glasses with high ionic-conductivity. C. R. Hebd. Seances Acad. Sci., Ser. 293(8), 563-565.

Martin, S. M., Sills, J. A., 1991. ^{29}Si and ^{27}Al MASS-NMR studies of Li_2S+AI_2S_3+ SiS_2 glasses. J. Non-Cryst. Solids 135, 171-181.

Mercier, R., Malugani, J. P., Fahys, B., Robert, G., 1981. Superionic conduction in Li_2S-P_2S_5-LiI- glasses. Solid State Ionics 5, 663-666.

Michel-Lledos, V.; Pradel A.; Ribes, M.; 1992. Lithium conductive selenide glasses. European journal of solid state and inorganic chemistry 29 (2), 301-310.

Moran, K., Shibao, R., Eckert, H., 1990. Structural tailoring of silicon chalcogenide glasses: Compositional control of edge-sharing units as monitored by high-resolution ^{29}Si solid state NMR. Hyperfine Interactions 62, 55-64.

667 Morimoto, H., Yamashita, H., Tatsumisago, M., Minami, T., 1999. Mechanochemical synthesis
668 of new amorphous materials of $60Li_2S{\cdot}40SiS_2$ with high lithium ion conductivity. J. Am.
669 Ceram. Soc. 82 (5) 1352-1354.
670 Olivier-Fourcade, J., Philippot, E., Ribes, M., Maurin, M., 1972. Étude structurale d'un
671 thiogermanate de sodium a chaines infinies $(Na_2GeS_3)_n$. Caractérisation dans le binaire
672 Na_2S- GeS_2. Rev. Chim. Miner. 9, 757-770.
673 Olivier-Fourcade, J., Jumas, J.C., Ribes, M., Philippot, E., Maurin, M., 1978. Evolution
674 structurale et nature des liaisons dans la série des composés soufrés du silicium, du
675 germanium, et de l'étain. J. Solid State Chem. 23 (1-2), 155-176.
676 Otto, K., 1966. Electrical conductivity of SiO2-B2O3 glasses containing lithium or sodium.
677 Phys. Chem. Glasses 7(1), 29-37.
678 Peters, J., Krebs, B., 1982. Silicon disulphide and silicon diselenide: a reinvestigation. Acta
679 Cryst. B38, 1270-1272.
680 Porod, G., 1982. Small angle X-ray scattering; Glatter, O., Kratky, O., Eds.; Academic Press,
681 New York, pp. 17-51.
682 Pradel, A., Pagnier, T., Ribes, M., 1985. Effect of rapid quenching on electrical properties of
683 lithium conductive glasses. Solid State Ionics 17 (2), 147-154.
684 Pradel, A., Ribes M., 1986. Electrical properties of lithium conductive silicon sulfide glasses
685 prepared by twin roller quenching. Solid State Ionics 18 & 19, 351-355.
686 **Pradel, A., Ribes M., 1989. Ionic conductive glasses. Materials Science and Engineering**
687 **B3, 45-56. (Pradel, 1989a)**
688 Pradel, A., Ribes, M., 1989. Lithium chalcogenide conductive glasses. Materials Chemistry and
689 Physics 23 (1-2), 121-142. **(Pradel, 1989b)**
690 Pradel, A., Ribes, M., 1992. Ionically conductive chalcogenide glasses. J. Solid State Chem.
691 96, 247-257. (Pradel, 1992a)
692 Pradel, A., Michel-Lledos, V., Ribes, M., 1992. Structural and electrical characterization of
693 glasses in the system Li_2Se-$SiSe_2$ by ^{29}Si MAS NMR and Raman spectroscopy. Solid State
694 Ionics 53-56, 1187-1193. (Pradel, 1992b)
695 Pradel, A., Michel-Lledos, V., Ribes, M., Eckert, H., 1993. Two New Polymorphs of $SiSe_2$:
696 Structural Investigation by Raman and ^{29}Si MAS NMR Spectroscopies and Relationship
697 with the Structure of Vitreous $SiSe_2$. Chem. Mater. 5, 377-380.
698 Pradel, A., Ribes, M., 1994. Ion transport in superionic conducting glasses. J. Non-Cryst. Solids
699 172-174, 1315-1323.

Pradel, A., Taillades, G., Ribes, M., Eckert, H., 1995. ^{29}Si NMR structural studies of ionically conductive silicon chalcogenide glasses and model compounds. J. Non-Cryst. Solids 188 (1-2), 75-86.

Pradel, A., Rau, C., Bittencourt, D., Armand, P., Philippot, E., Ribes, M., 1998. Mixed glass former effect in the system $0.3Li_2S$-$0.7[(1-x)SiS_2$-$xGeS_2]$: A Structural Explanation. Chem. Mater. 10, 2162-2166.

Rau, C., Armand, P., Pradel, A., Varsamis, C. P. E., Kamitsos, E. I., Granier, D., Ibanez, A., Philippot, E., 2001. Mixed cation effect in chalcogenide glasses Rb_2S-Ag_2S-GeS_2. Phys. Rev. B 63, 184204.

Ravaine, D., Souquet, J.L., 1977. A thermodynamic approach to ionic conductivity in oxide glasses.1. Correlation of the ionic conductivity with the chemical potential of alkali oxide in oxide glasses. Phys. Chem. Glasses18, 27-31.

Ribes, M., Ravaine, D., Souquet, J.L., Maurin. M., 1979. Synthese, structure, et conduction ionique de nouveaux verres à base de sulfures. Rev. Chim. Miner. 16, 339-348.

Robinel, E., Carette, B., Ribes, M., 1983. Silver sulfide based glasses (I). Glass forming regions, structure and ionic conduction of glasses in GeS_2-Ag_2S and GeS_2-Ag_2S-AgI systems. J. Non-Cryst. Solids 57, 49-58

Sahami, S., Shea, S. W., Kennedy, J. H., 1985. Preparation and conductivity measurements of SiS_2-Li_2S-LiBr lithium ion conductive glasses. J. Electrochem. Soc. 132, 985-986.

Schramm, C. M., Jong, B. H. W. S., Parziale, V. E., 1984. ^{29}Si Magic angle spinning NMR study on local silicon environments in amorphous and crystalline lithium silicates. J. Am. Chem. Soc. 106 (1984) 4396-4402.

Seo, I., Kim, Y., Martin, S.W., 2016. Characterization of thin-film electrolytes for all solid-state batteries. J. Alloys Compounds 661 245-250.

Shastri, A., Watson, D., Ding, Q.-P., Furukawa, Y., Martin, S.W., 2019. ^{23}Na nuclear magnetic resonance study of $yNa_2S+(1-y)[xSiS_2+(1-x)PS_{5/2}]$ glassy solid electrolytes. Solid State Ionics 340, 115013.

Souquet, J.L., Robinel, E., Barrau, B., Ribes, M., 1981. Glass formation and ionic conduction in the M_2S-GeS_2 (M = Li, Na, Ag) systems. Solid State Ionics 3-4, 317-321.

Sugai, S., 1986. Two-directional photoinduced crystallization in $GeSe_2$ and $SiSe_2$ glasses. Phys. Rev. Lett. 57, 456.

Sugai, S., 1987. Stochastic random network model in Ge and Si chalcogenide glasses. Phys. Rev. B 35, 1345.

733 Tatsumisago, M., Hirai, K., Hirata, T., Takahashi, M., Minami, T., 1996. Structure and
734 properties of lithium ion conducting oxysulfide glasses prepared by rapid quenching. Solid
735 State Ionics 86-88, 487-490.
736 Tenhover, M., Hazle, M. A., Grasselli, R. K., Tompson, C. W., 1983. Chemical bonding and
737 the atomic structure of Si_xSe_{1-x} glasses. Phys. Rev. B 28, 4608. (Tenhover, 1983a)
738 Tenhover, M., Hazle, M. A., Grasselli, R. K., 1983. Atomic structure of SiS_2 and $SiSe_2$ glasses.
739 Phys. Rev. Lett. 51, 404. (Tenhover, 1983b)
740 Tenhover, M., Henderson, R.S., Lukco, D., Hazle, M.A., Grasselli, R.K., 1984. Vibrational
741 studies of crystalline and glassy $SiSe_2$. Solid State Communications 51(7), 455-459.
742 Tenhover, M., Harris, J.H., Hazle, M.A., Scher, H., Grasselli, R.K., 1985. Isoelectronic
743 substitution in $Si(S_xSe_{1-x})_2$ glasses. J. Non-Cryst. Solids 69 (2-3), 249-259.
744 Tenhover, M., Boyer, R.D., Henderson, R.S., Hammond, T.E., Shreve, G.A., 1988. Magic angle
745 spinning ^{29}Si nuclear magnetic resonance of Si-chalcogenide glasses. Solid State
746 Communications 65 (12), 1517-1521.
747 **Verweij, H., Buster, J.H.J.M., Remmers, G.F., 1979. Refractive index and density of Li-,**
748 **Na- and K-germanosilicate glasses. J. Mater.Sc. 14, 931-940.**
749 Visco, S. J., Spellane, P. J., Kennedy, J. H., 1985. Complex plane and ^{7}Li NMR studies of
750 arsenic sulfide-based lithium glasses. J. Electrochem. Soc. 132(7), 1766-1770.
751 Watson, D.E., Martin, S.W., 2017. Short range order characterization of the Na_2S+SiS_2 glass
752 system using Raman, infrared and ^{29}Si magic angle spinning nuclear magnetic resonance
753 spectroscopies. J. Non-Cryst. Solids 471, 39-50.
754 Watson, D. E., Martin, S.W., 2018. Structural characterization of the short-range order in high
755 alkali content sodium thiosilicophosphate glasses. Inorg. Chem. 57, 72-81. (Watson, 2018a)
756 Watson, D.E., Martin, S.W., 2018. Composition dependence of the glass-transition temperature
757 and molar volume in sodium thiosilicophosphate glasses: A structural interpretation using a
758 real solution model. J. Phys. Chem. B (122), 10637-10646. (Watson, 2018b)
759 Weiss, Al., Weiss, A., 1952. Die Kristallstruktur des Siliciumdiselenids. Z. Naturforsch 7b,
760 483-484.
761 Weiss, A., Rocktäschel, G., 1960. Zur Kenntnis von Thiosilicaten. Und Allg. Chemie 307 (1-
762 2), 1-6.
763 **Yoshiyagawa, M., Tomozawa, M., 1982. Electrical properties of rapidly-quenched lithium**
764 **silicate glasses. J. Phys. Colloque C9, 411-414.**
765 Zhao, R., Kmiec, S., Hu, G., Martin, S.W., 2020. Lithium thiosilicophosphate glassy solid
766 electrolytes synthesized by high-energy ball-milling and melt-quenching: Improved

suppression of lithium dendrite growth by Si doping. ACS Appl. Mater. Interfaces 12, 2327-2337.

Zhang, Z., Kennedy, J. H., 1990. Synthesis and characterization of the B_2S_3-Li_2S, the P_2S_5-Li_2S and the B_2S_3-P_2S_5-Li_2S glass systems. Solid State Ionics 38 (3-4), 217-224.

Zintl, E., Loosen, K., 1935. Siliciumdisulfid, ein anorganischer faserstoff mit kettenmolekülen. Z. Phys. Chem. Leipzig 174 (1), 301-311.

Figure captions

Figure 1: Basic building blocks of SiO_2-quartz, crystalline SiS_2 and 700-$SiSe_2$. In the middle, tentative structural model for crystalline 400-$SiSe_2$. O atoms are represented by red spheres, and S and Se atoms are represented by light green spheres.

Figure 2: ^{29}Si MAS NMR spectra of $SiSe_2$ polymorphs and $SiSe_2$ glass. Spinning sidebands are indicated by asterisks.

Figure 3: Possible Si environments in alkali thiosilicate and selenosilicate compounds.

Figure 4: Schematic representation of a cross-linked chain-cluster (CLCC) proposed by Griffiths and collaborators (Griffiths 1984)

Figure 5: ^{29}Si MAS NMR spectra for xLi_2S-$(1-x)SiS_2$ glasses.

Figure 6: XPS S_{2p} core peaks for xLi_2S-$(1-x)SiS_2$ glasses. Doublet 1: NBS; doublet 2: BS.

Figure 7: ^{29}Si MAS NMR spectra for xLi_2Se-$(1-x)SiSe_2$ glasses. Spinning sidebands are indicated by asterisks.

Figure 8: Deconvolution of the ^{29}Si MAS-NMR spectrum of $0.6Na_2Se$-$0.4SiSe_2$ glass. Bottom: experimental spectrum; top: simulated spectrum assuming the chemical shifts and population distribution given in inset. Expected population distributions for statistical and chemically ordered models are also given.

Figure 9: Glass transition temperatures in glasses xM_2X-$(1-x)SiX_2$ with M= Li, Na, Ag and X = S, Se. The dashed lines are a guideline for experimental data.

Figure 10: Conductivity σ and activation energy of conductivity E_σ for xLi_2X-$(1- x)SiX_2$ glasses (X = O, S and Se).

Figure 11: ^{29}Si MAS NMR spectra for $0.5(xNa_2S$-$(1-x)Li_2S)$-$0.5SiS_2$ glasses.

Figure 12: (a) Conductivity σ and activation energy of conductivity E_σ and (b) glass transition temperature, T_g and activation energy of the relaxation time T_1, E_{T1} for $0.5[xNa_2S\text{-}(1\text{-}x)Li_2S]\text{-}0.5SiS_2$ glasses. The dashed lines are guidelines for experimental data.

Figure 13: Glass formation region in the $Li_2S\text{-}Al_2S_3\text{-}SiS_2$ system. Circles and triangles correspond to glasses, while stars refer to partially crystallized samples.

Figure 14: Raman spectra of $0.5\ Li_2S\text{-}xAl_2S_3\text{-}(0.5\text{-}x)SiS_2$ glasses, (Si-S) and ($Si\text{-}S^-$) stand for bridging Si-S bonds and non-bridging $Si\text{-}S^-$ bonds, respectively. Raman spectra of crystalline SiS_2 and $\alpha\text{-}Al_2S_3$ are reported for comparison.

Figure 15: Conductivity σ, activation energy of conductivity E_σ and glass transition temperature T_g of $0.5Li_2S\text{-}xAl_2S_3\text{-}(0.5\text{-}x)SiS_2$ glasses elaborated by twin-roller quenching. The dashed lines are guidelines for experimental data.

Figure 16: Investigated glass compositions in the system $Li_2S\text{-}SiS_2\text{-}GeS_2$, i.e. $0.3Li_2S\text{-}0.7[(1\text{-}x)SiS_2\text{-}xGeS_2]$ and $0.5Li_2S\text{-}0.5[(1\text{-}x)SiS_2\text{-}xGeS_2]$.

Figure 17: Raman spectra of $0.3Li_2S\text{-}0.7[(1\text{-}x)SiS_2\text{-}xGeS_2]$ glasses. (Si(Ge)-S) and ($Si(Ge)\text{-}S^-$) stand for bridging Si(Ge)-S bonds and non-bridging $Si(Ge)\text{-}S^-$ bonds, respectively. Blue dashed line corresponds to the main peak of $0.5Li_2S\text{-}0.5SiS_2$ glass. Raman spectrum of crystalline GeS_2 is reported for comparison. SAXS intensity for five glasses belonging to the three different regions is shown in the inset.

Figure 18: Glass transition temperature, T_g, density, ρ, for $Li_2S\text{-}SiS_2\text{-}GeS_2$ glasses. Filled and empty symbols correspond to series $0.3Li_2S\text{-}0.7[(1\text{-}x)SiS_2\text{-}xGeS_2]$ and $0.5Li_2S\text{-}0.5[(1\text{-}x)SiS_2\text{-}xGeS_2]$, respectively. The inset displays the DSC curve of $0.3Li_2S\text{-}0.25SiS_2\text{-}0.45GeS_2$ glass. The dashed lines are guidelines for experimental data.

Figure 19: Conductivity σ and activation energy of conductivity E_σ for $Li_2S\text{-}SiS_2\text{-}GeS_2$ glasses. Filled and empty symbols correspond to series $0.3Li_2S\text{-}0.7[(1\text{-}x)SiS_2\text{-}xGeS_2]$ and $0.5Li_2S\text{-}0.5[(1\text{-}x)SiS_2\text{-}xGeS_2]$, respectively. The dashed lines are guidelines for experimental data.

Figure 20: Investigated glass compositions in the system Na_2S-SiS_2-$PS_{5/2}$, i.e. $0.5Na_2S$-$0.5[xSiS_2$-$(1-x)PS_{5/2}]$ and $0.67Na_2S$-$0.33[xSiS_2$-$(1-x)PS_{5/2}]$ (purple symbols) and line of investigated compositions in the Li_2S-SiS_2-P_2S_5 system, i.e. glasses with 60 mol% Li_2S.

Figure 21: Composition dependence of the fractions of the P Qn and Si Qn species existing in the $0.5Na_2S+0.5[xSiS_2+(1-x)PS_{5/2}]$ glass system. P Q0, P Q1 and P Q2 entities are shown at the top. P, S and Na atoms are represented by pink, green and light orange spheres, respectively. P' Q1 stands for a P Q1 species with a P-P bond. Lines are only guidelines.

Figure 22: Glass transition temperature T_g, molar volume, and fraction of bridging sulfur (BS/(BS + NBS)) in the $0.5Na_2S+0.5[xSiS_2+(1-x)PS_{5/2}]$ glass system. The dashed lines are guidelines for experimental data.

Figure 23: Composition dependence of the fractions of the main B Qn and Si Qn units in $0.6Na_2S+0.4[xBS_{3/2}+(1-x)SiS_2]$ glasses. In the inset is shown the line of studied compositions.

Figures

Figure 1

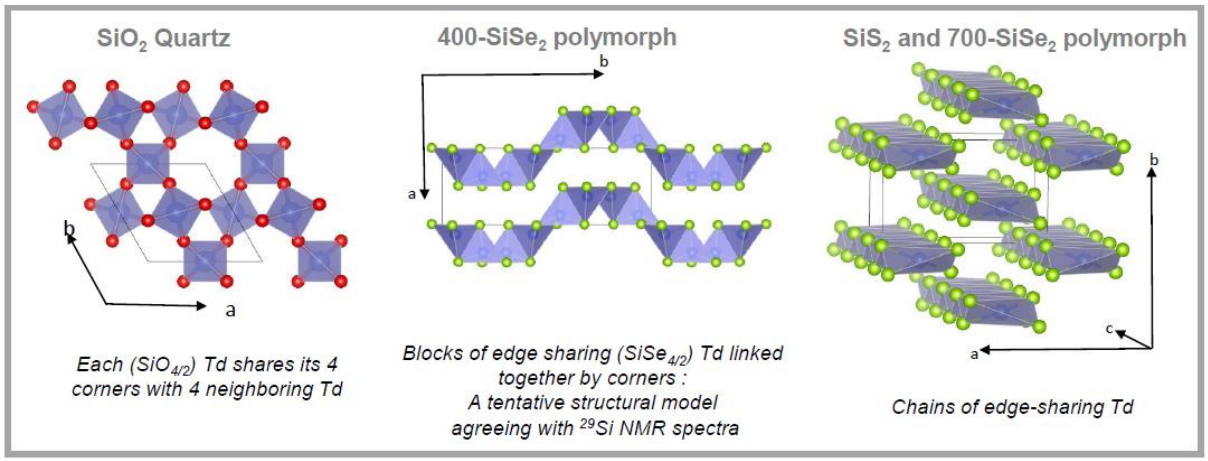

Figure 2

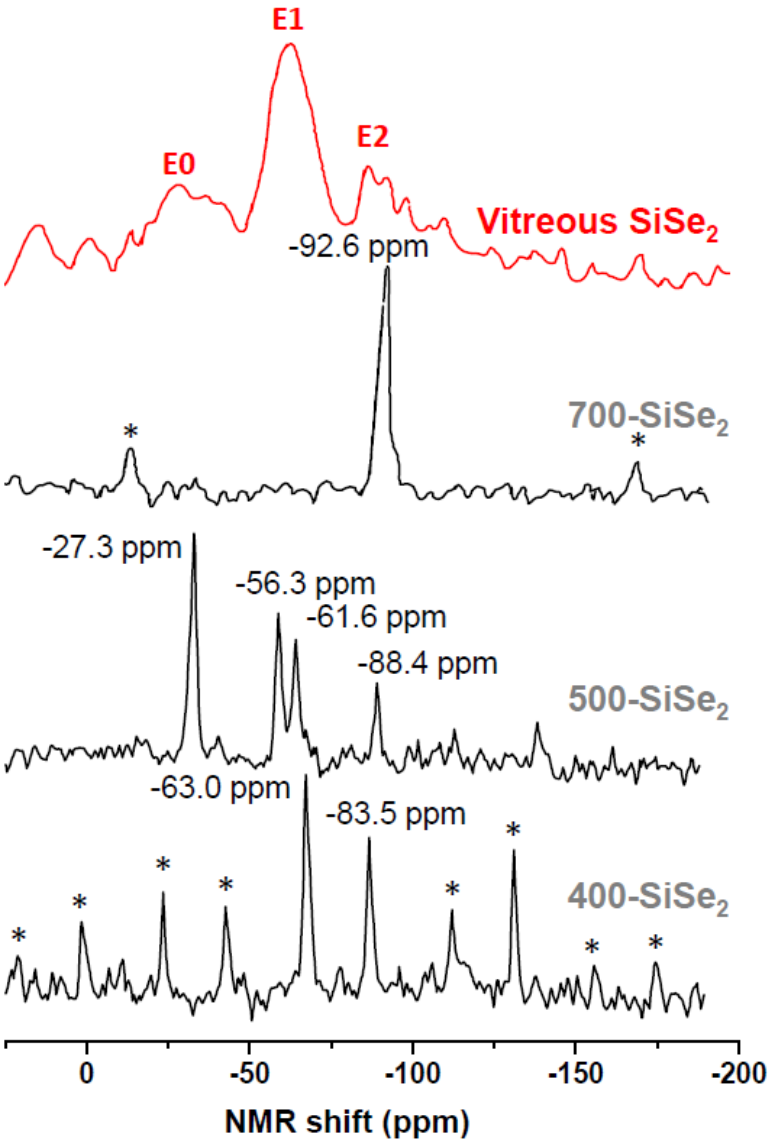
E1
E0
E2
Vitreous SiSe2
-92.6 ppm
700-SiSe2
-27.3 ppm
-56.3 ppm
-61.6 ppm
-88.4 ppm
500-SiSe2
-63.0 ppm
-83.5 ppm
400-SiSe2
0
-50
-100
-150
-200
NMR shift (ppm)

Figure 3

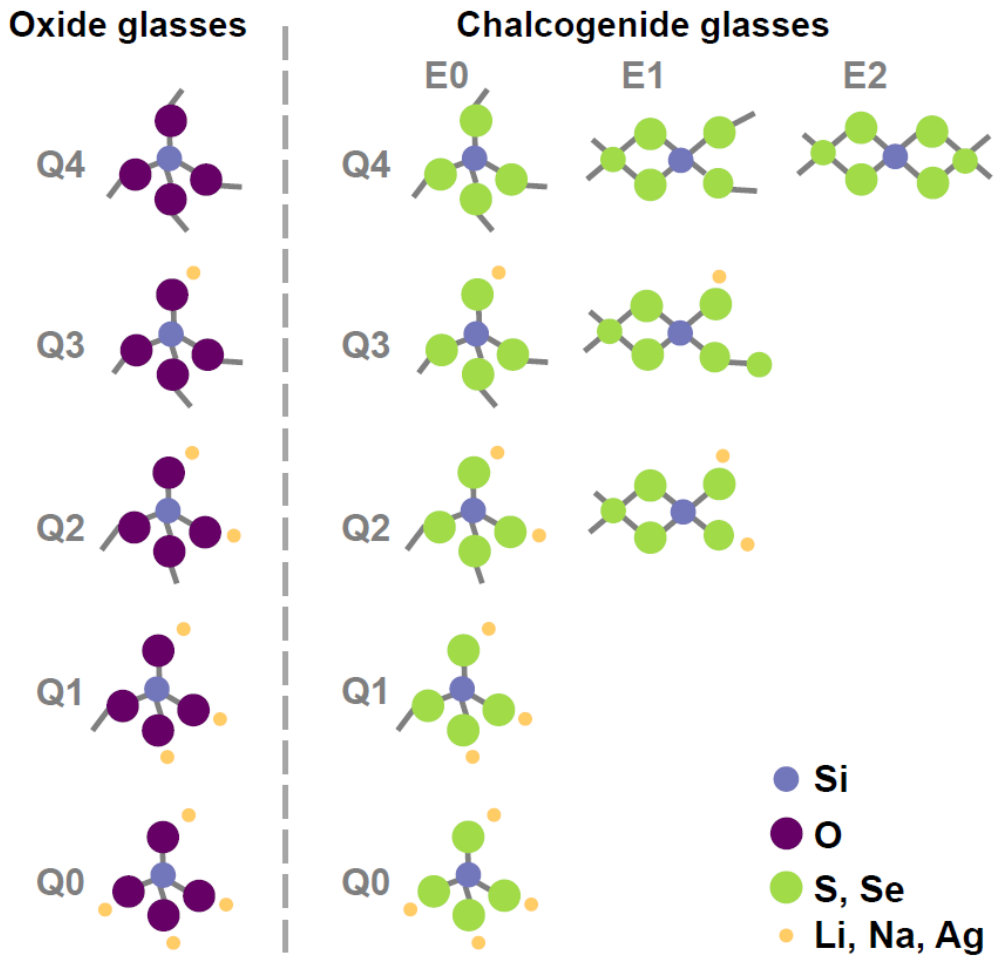
Oxide glasses
Chalcogenide glasses
E0
E1
E2
Q4
Q3
Q2
Q1
Q0
Si
O
S, Se
Li, Na, Ag

Figure 4

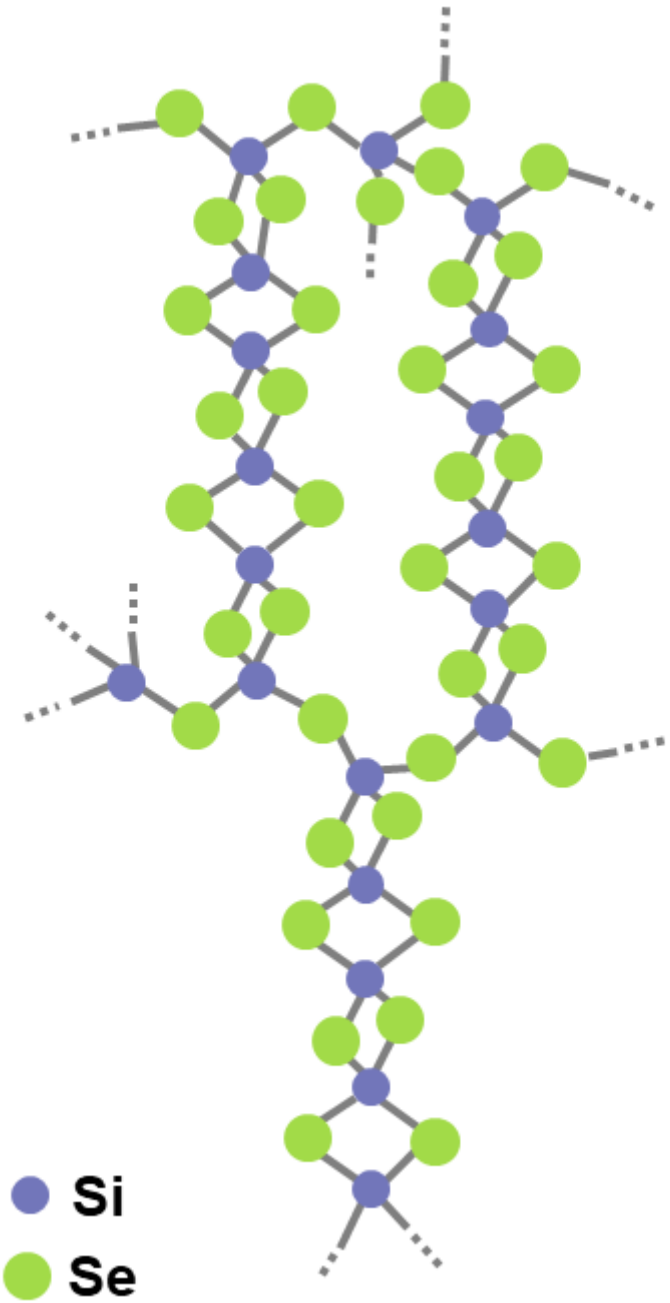

883 **Figure 5**

884

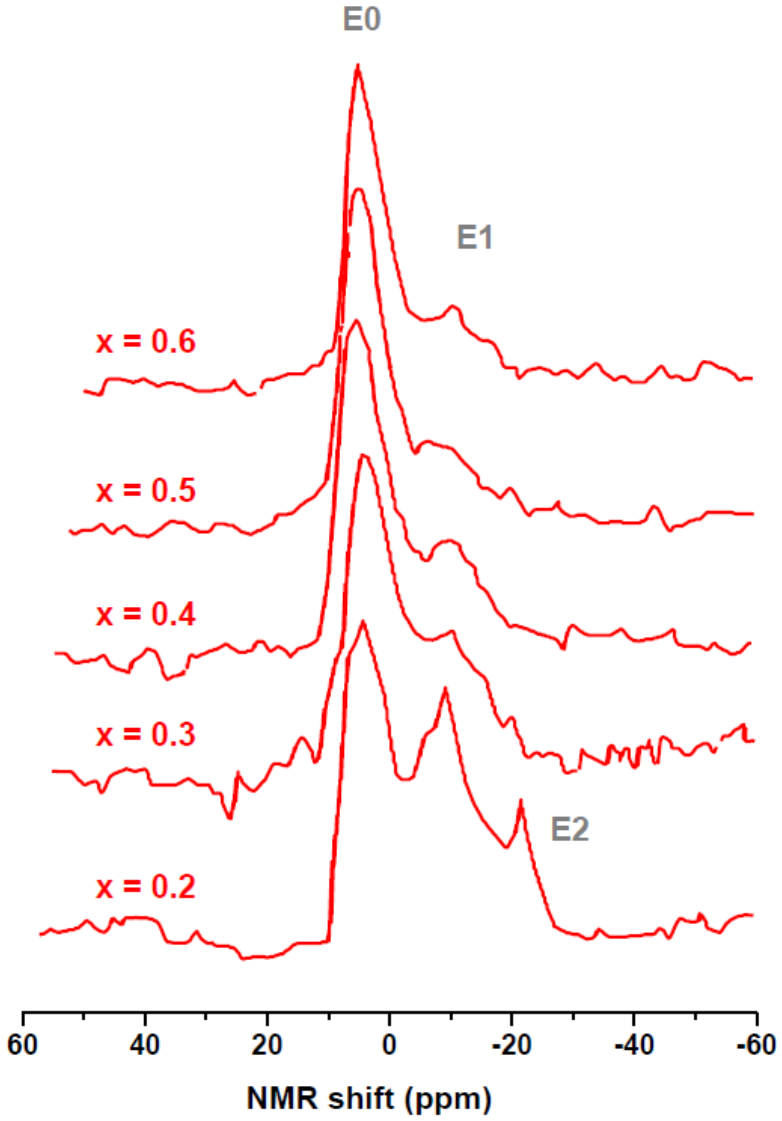

885

886

887 **Figure 6**

888

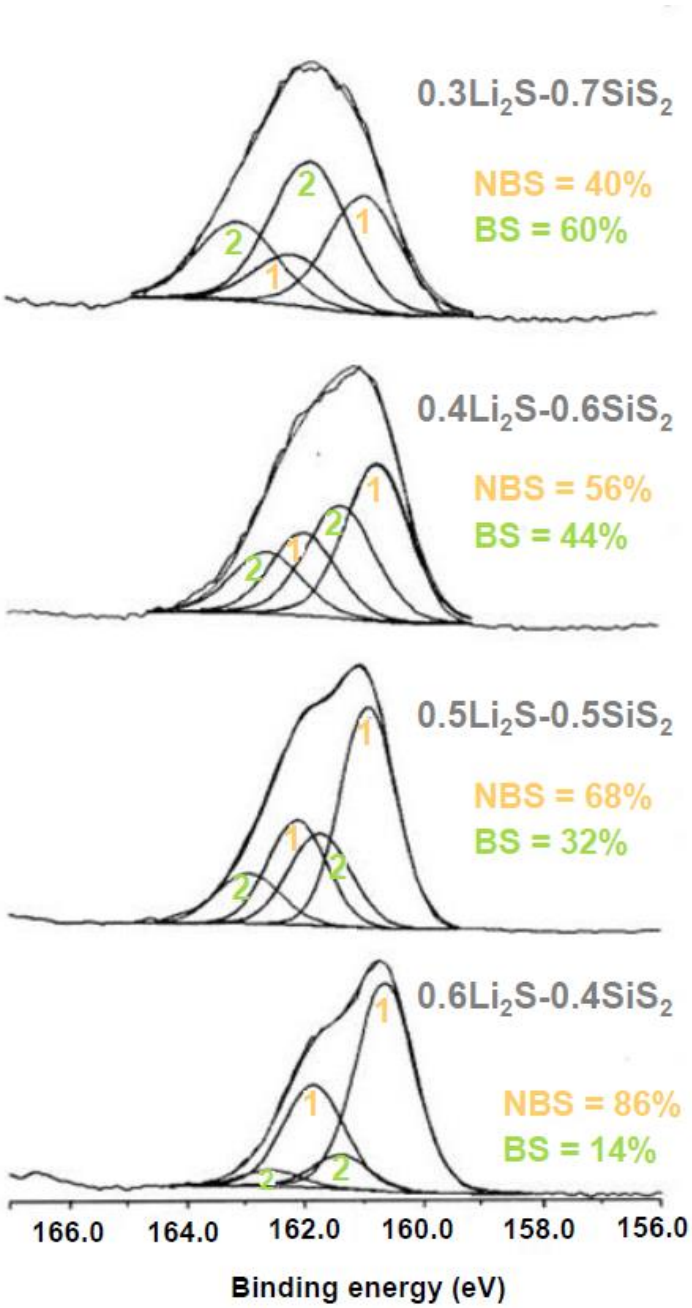

889

890

Figure 7

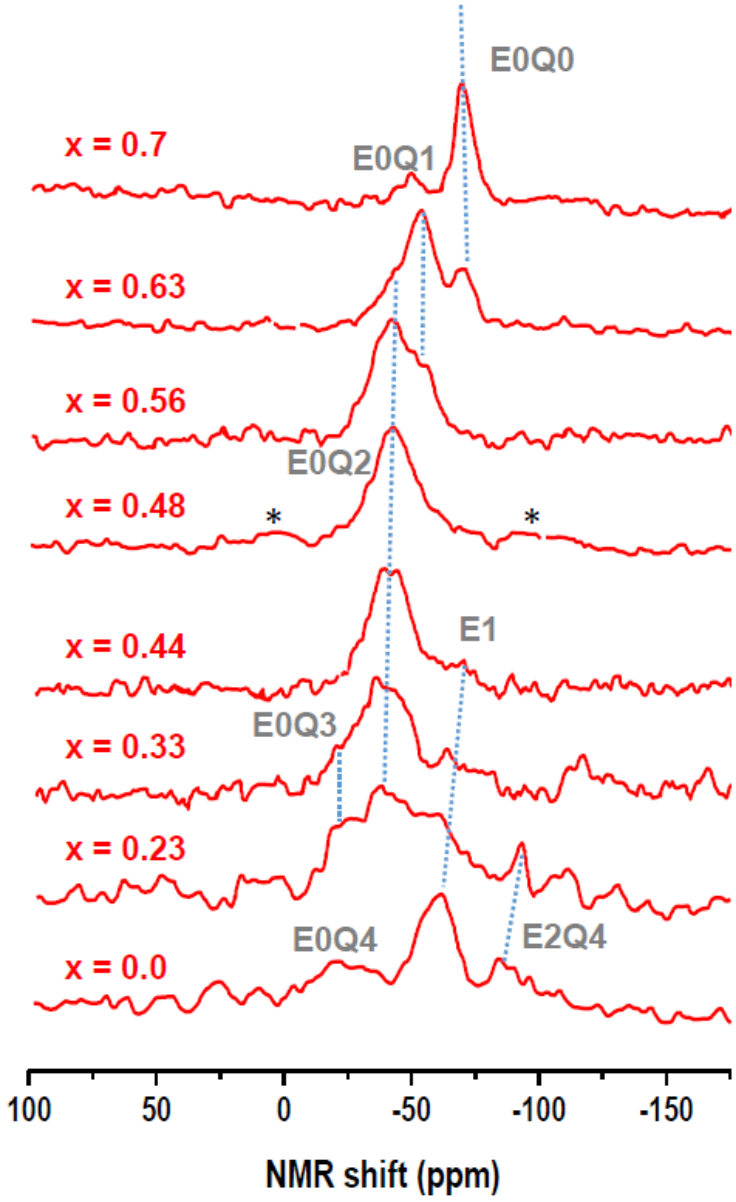
E0Q0
x = 0.7
E0Q1
x = 0.63
x = 0.56
E0Q2
x = 0.48
*
*
E1
x = 0.44
E0Q3
x = 0.33
x = 0.23
E0Q4
E2Q4
x = 0.0
100
50
0
-50
-100
-150
NMR shift (ppm)

Figure 8

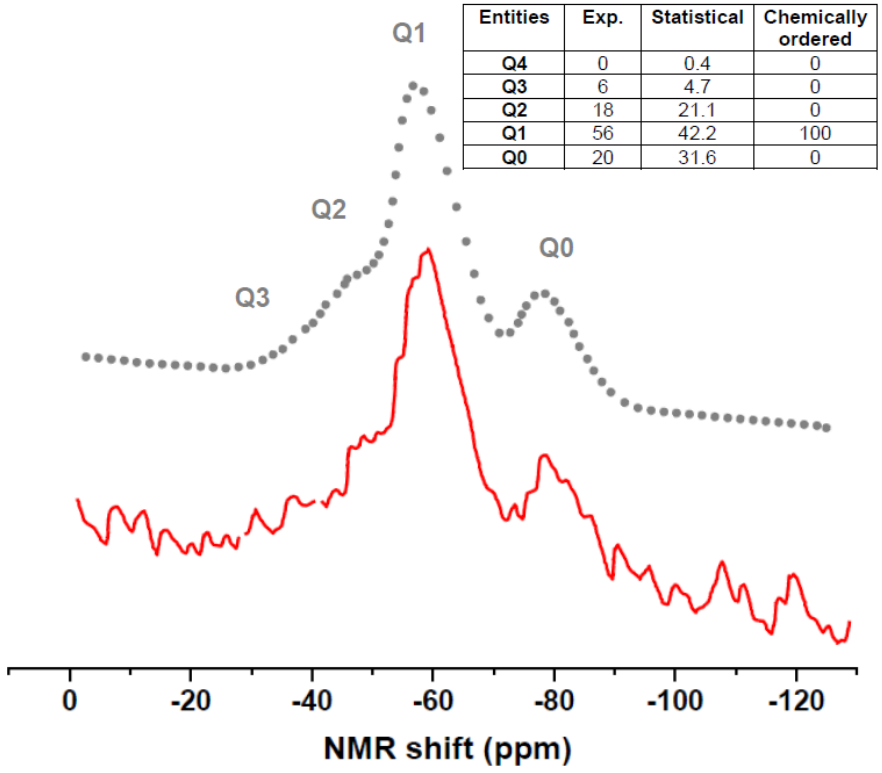

Entities	Exp.	Statistical	Chemically ordered
Q4	0	0.4	0
Q3	6	4.7	0
Q2	18	21.1	0
Q1	56	42.2	100
Q0	20	31.6	0

899 **Figure 9**

900

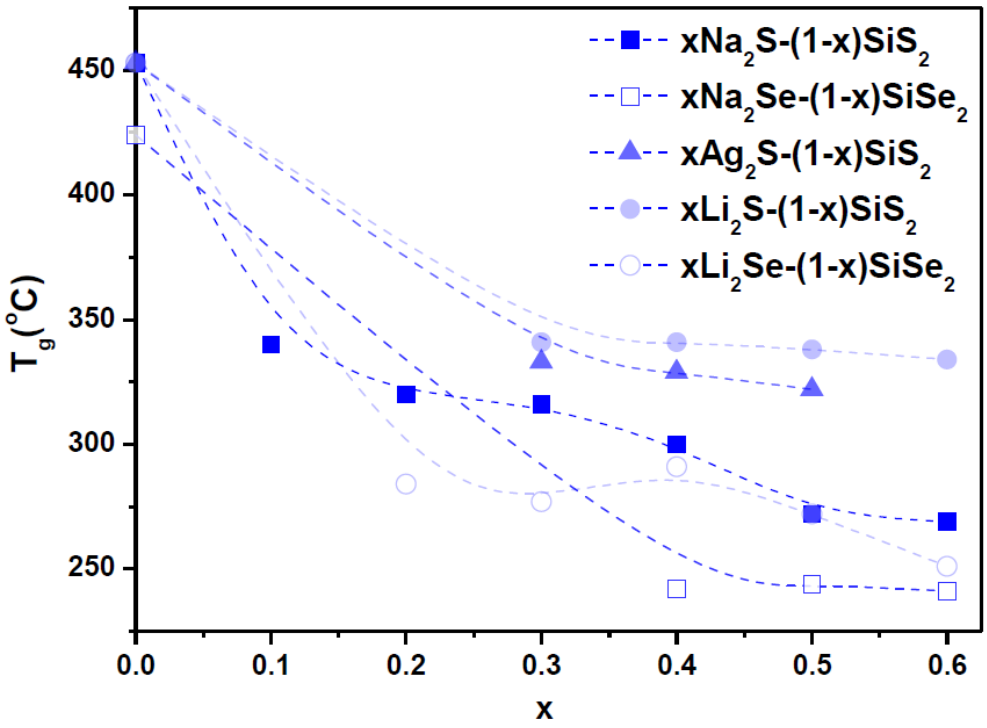

901

902

Figure 10

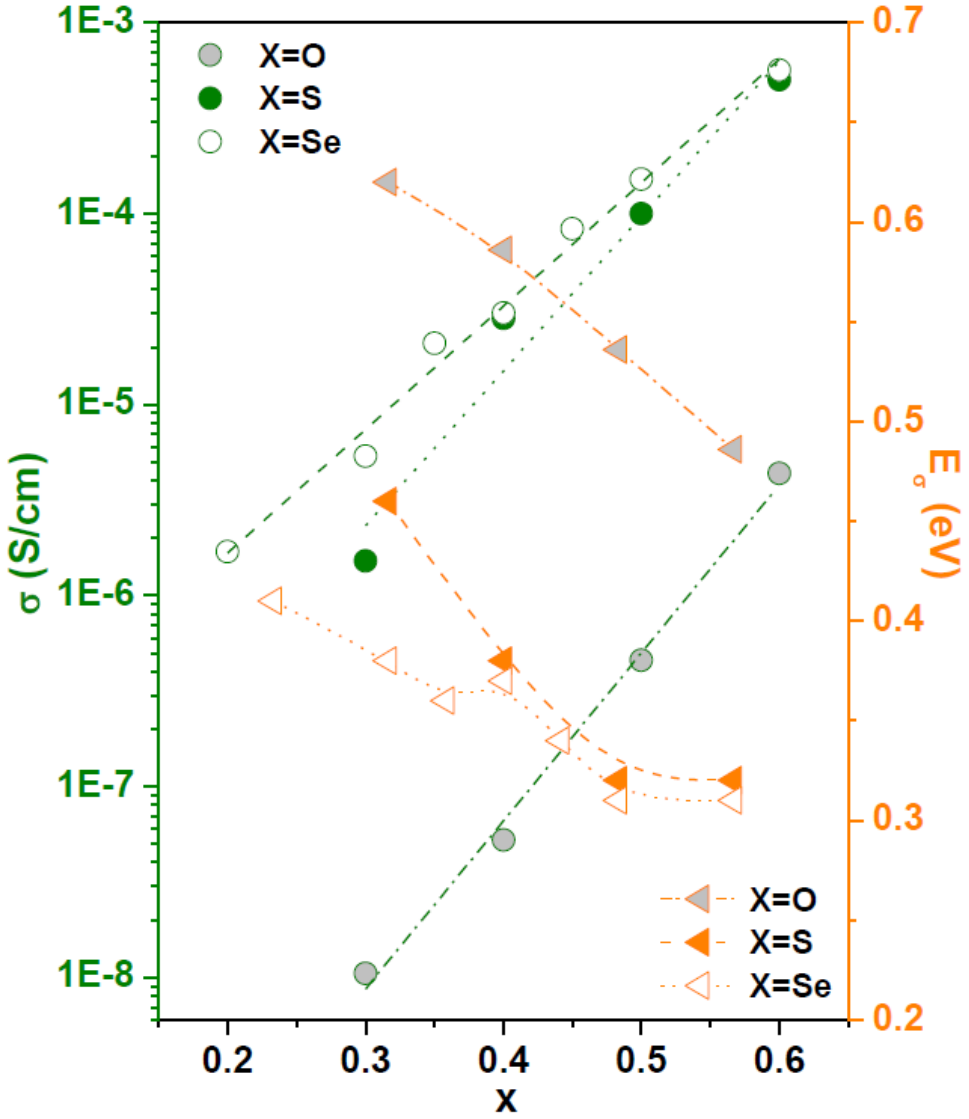
1E-3
1E-4
1E-5
1E-6
1E-7
1E-8
σ (S/cm)
0.7
0.6
0.5
0.4
0.3
0.2
E_σ (eV)
X=O
X=S
X=Se
X=O
X=S
X=Se
0.2
0.3
0.4
0.5
0.6
X

907 **Figure 11**

908

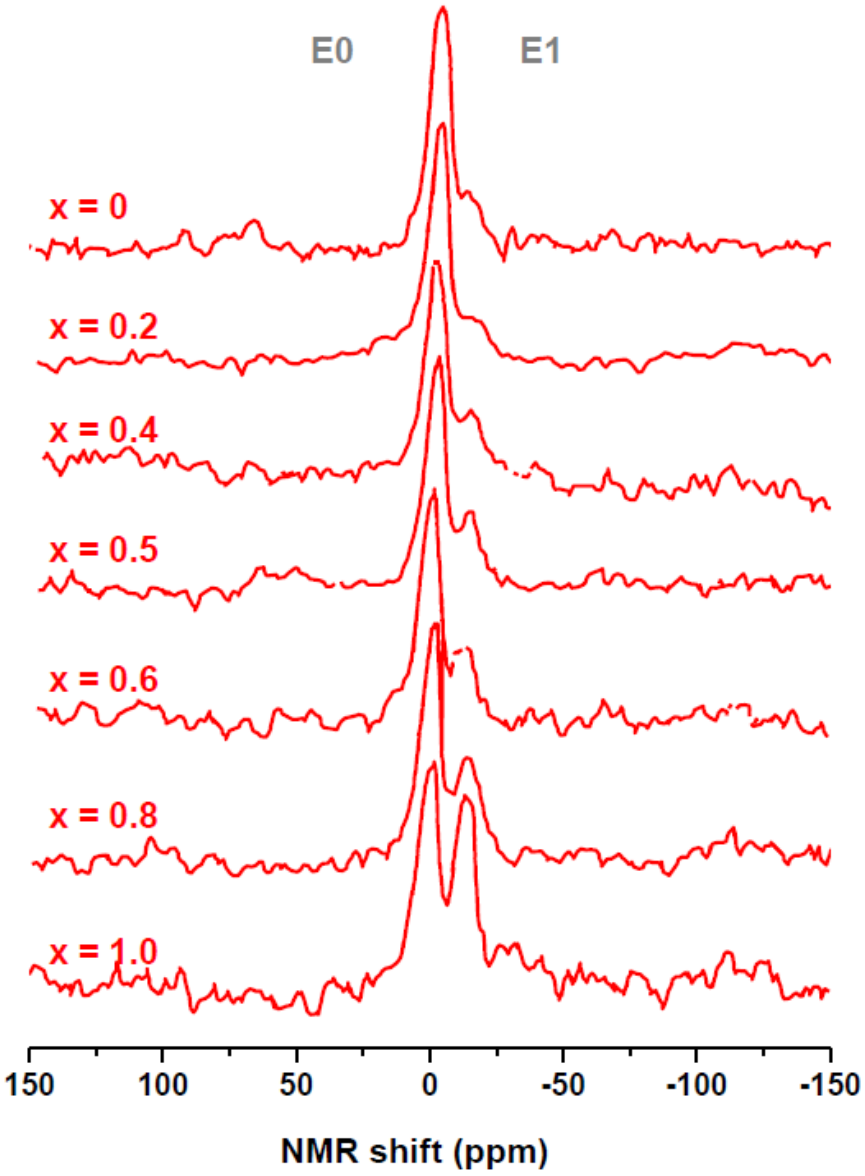

909

910

Figure 12

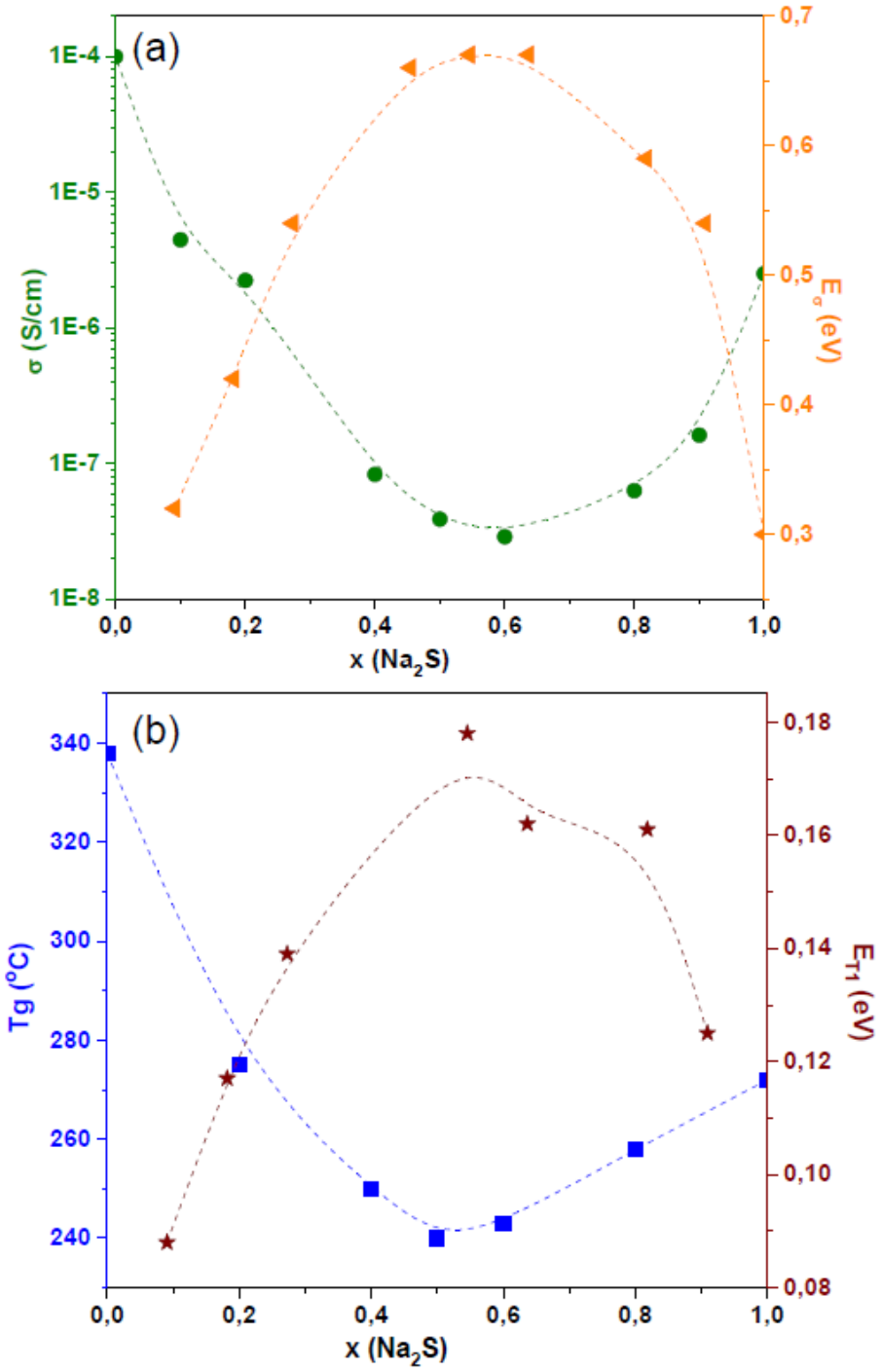
(a)
1E-4
1E-5
1E-6
1E-7
1E-8
σ (S/cm)
0,7
0,6
0,5
0,4
0,3
Eσ (eV)
0,0
0,2
0,4
0,6
0,8
1,0
x (Na2S)
(b)
340
320
300
280
260
240
Tg (°C)
0,18
0,16
0,14
0,12
0,10
0,08
ET1 (eV)
0,0
0,2
0,4
0,6
0,8
1,0
x (Na2S)

Figure 13

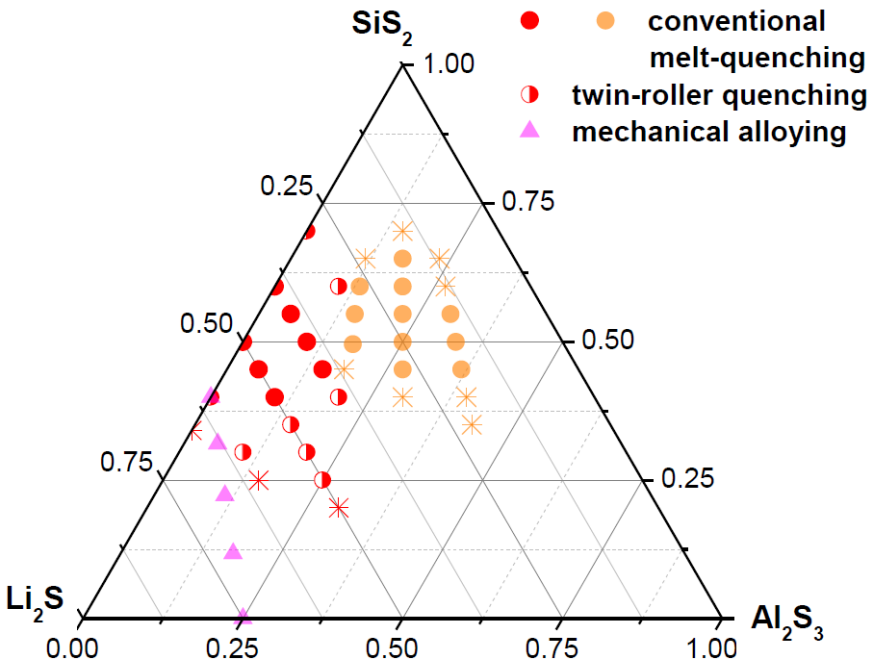
SiS2
Li2S
Al2S3
1.00
0.75
0.50
0.25
0.00
0.25
0.50
0.75
1.00
conventional melt-quenching
twin-roller quenching
mechanical alloying

Figure 14

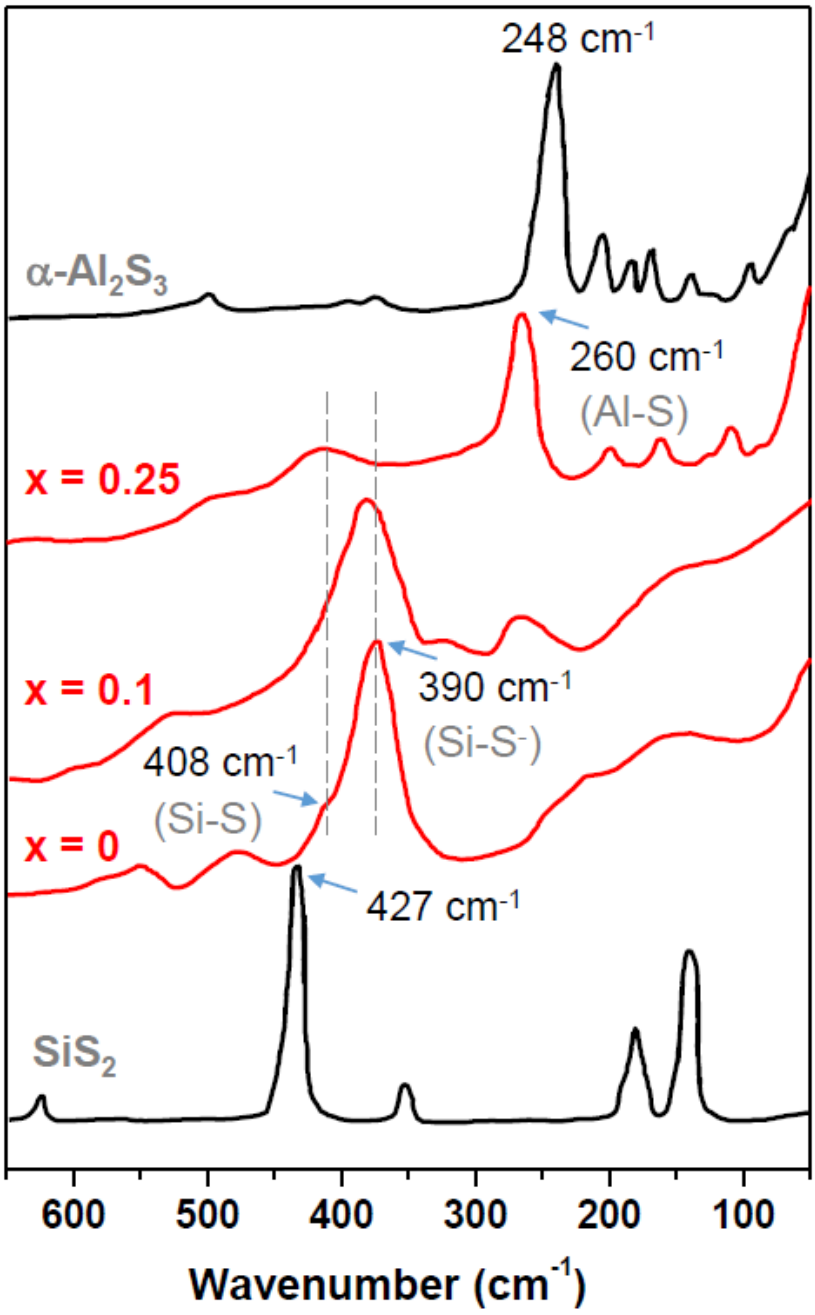
248 cm-1
α-Al2S3
260 cm-1
(Al-S)
x = 0.25
x = 0.1
390 cm-1
(Si-S-)
408 cm-1
(Si-S)
x = 0
427 cm-1
SiS2
600
500
400
300
200
100
Wavenumber (cm-1)

Figure 15

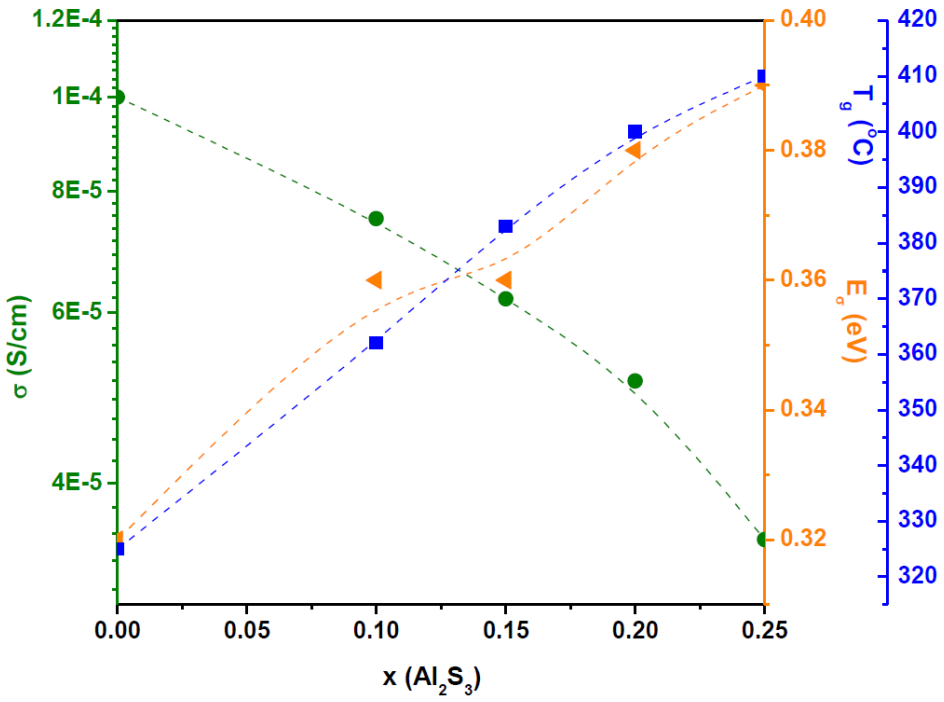
1.2E-4
1E-4
8E-5
6E-5
4E-5
σ (S/cm)
0.40
0.38
0.36
0.34
0.32
E_σ (eV)
420
410
400
390
380
370
360
350
340
330
320
T_g (°C)
0.00
0.05
0.10
0.15
0.20
0.25
x (Al2S3)

928 **Figure 16**

929

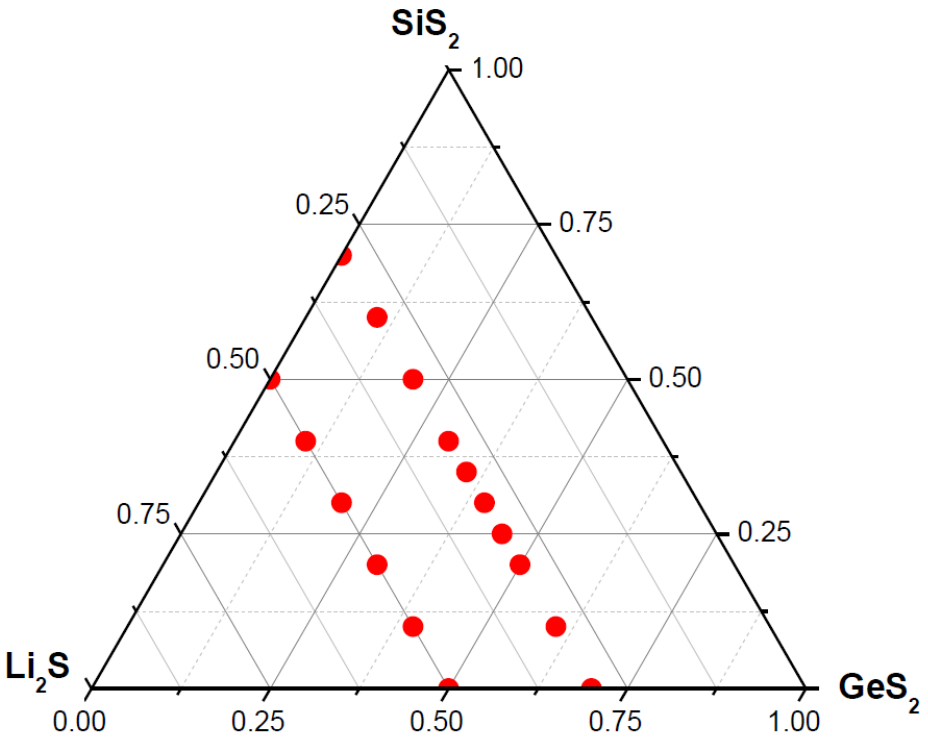

930

931

Figure 17

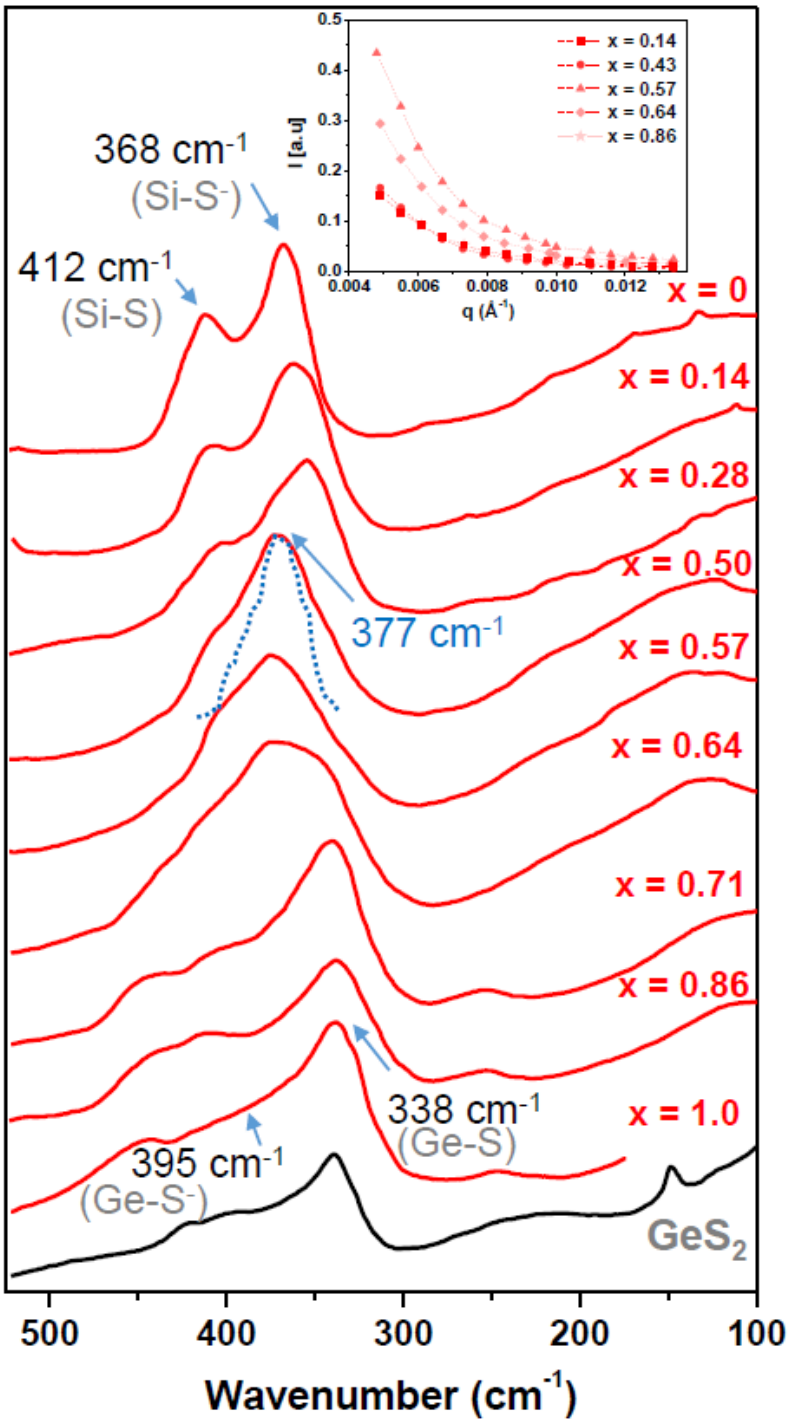
368 cm-1
(Si-S-)
412 cm-1
(Si-S)
377 cm-1
338 cm-1
(Ge-S)
395 cm-1
(Ge-S-)
x = 0
x = 0.14
x = 0.28
x = 0.50
x = 0.57
x = 0.64
x = 0.71
x = 0.86
x = 1.0
GeS2
500
400
300
200
100
Wavenumber (cm-1)
I [a.u]
q (Å-1)
0.004
0.006
0.008
0.010
0.012
0.0
0.1
0.2
0.3
0.4
0.5

Figure 18

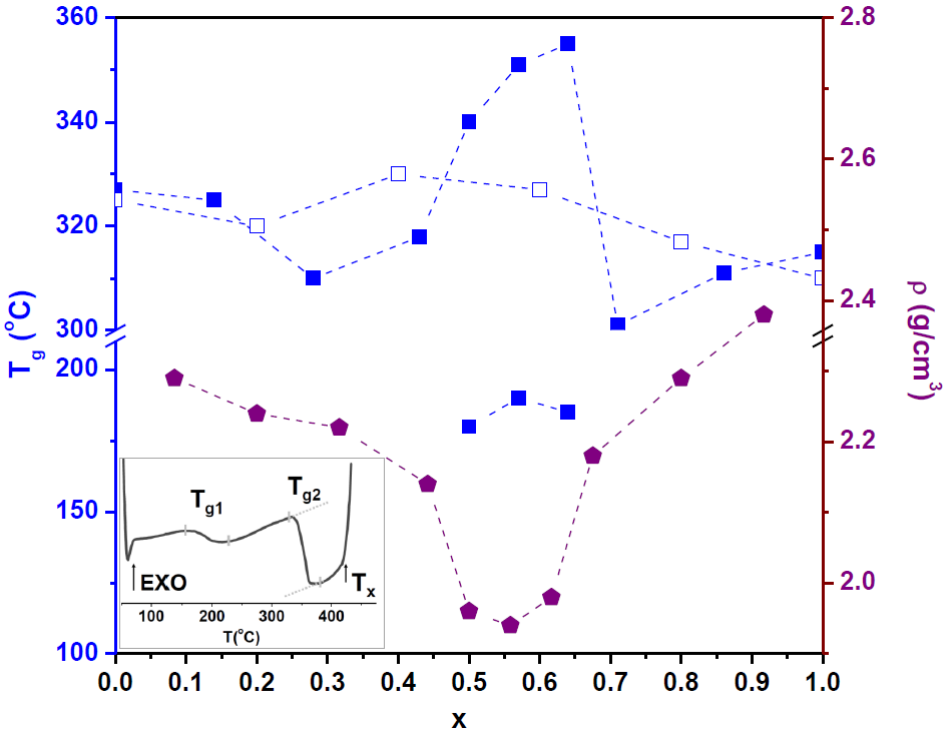
360
340
320
300
200
150
100
2.8
2.6
2.4
2.2
2.0
T_g (°C)
ρ (g/cm^3)
0.0
0.1
0.2
0.3
0.4
0.5
0.6
0.7
0.8
0.9
1.0
x
T_{g1}
T_{g2}
EXO
T_x
100
200
300
400
T(°C)

940 **Figure 19**

941

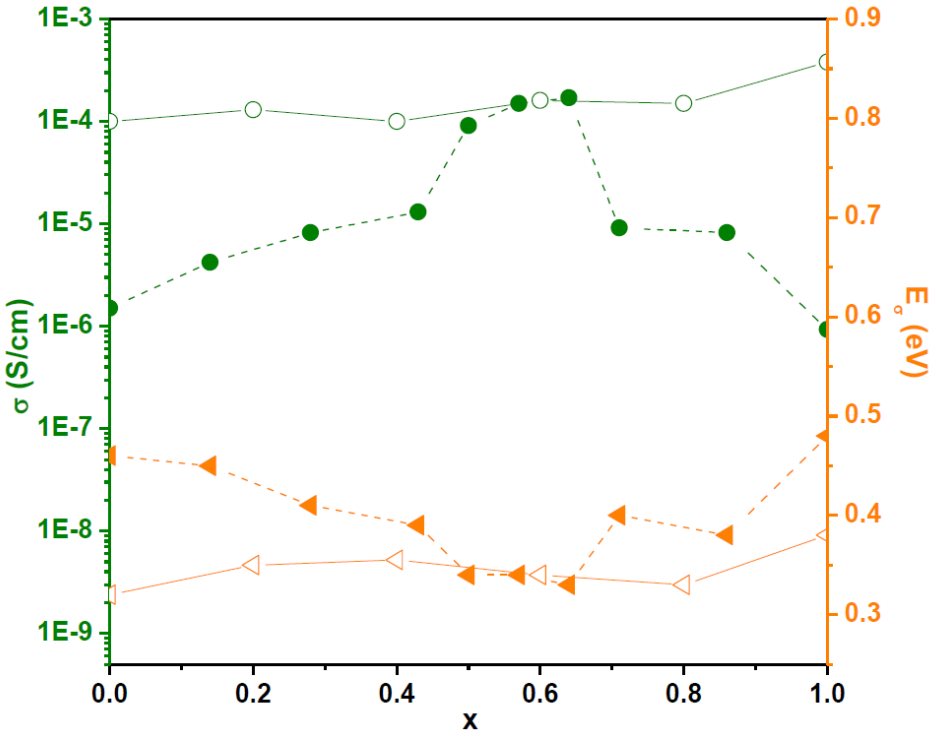

942

943

Figure 20

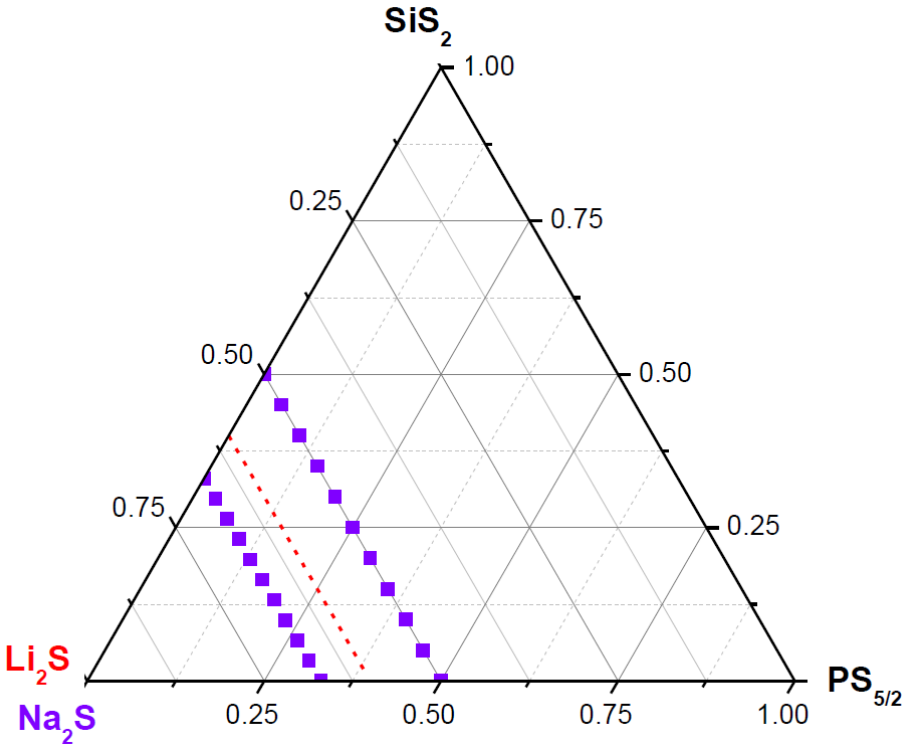

948 **Figure 21**

949

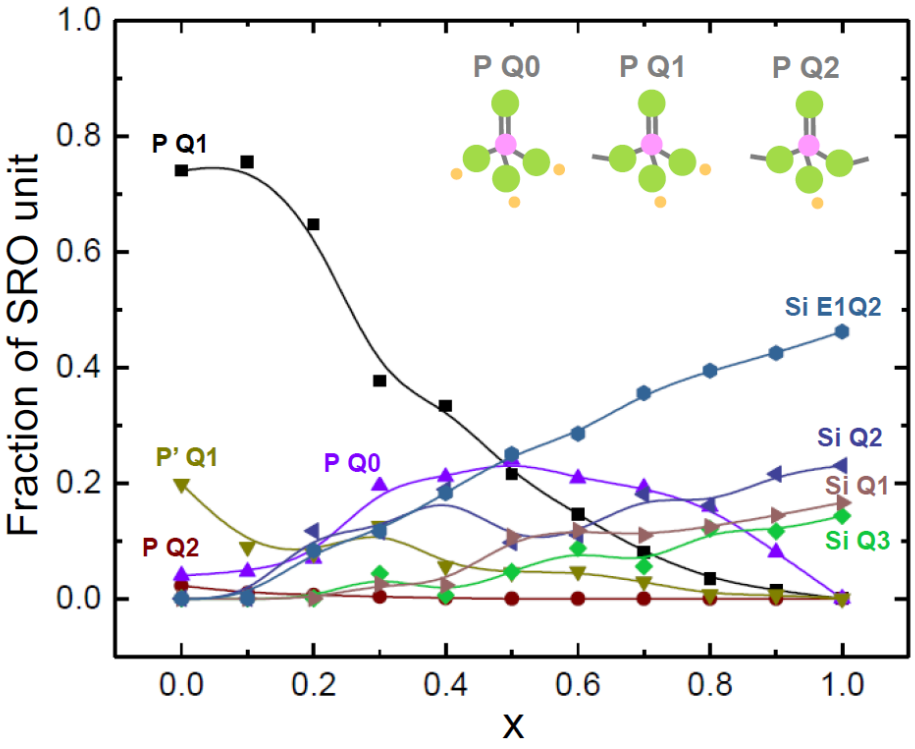

950

951

952 **Figure 22**

953

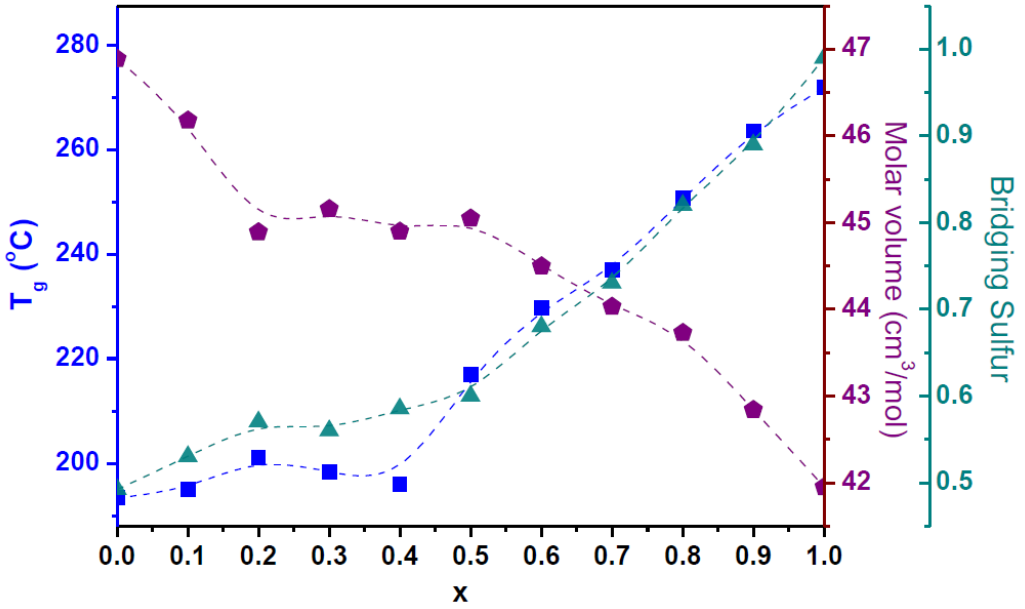

954

955

Figure 23